Localized Disturbances in a Flat Plate Boundary Layer

by

Jörgen Olsson

SUBMITTED TO THE DEPARTMENT OF
AERONAUTICS AND ASTRONAUTICS IN PARTIAL
FULFILLMENT OF THE REQUIREMENTS FOR THE
DEGREE OF

MASTER OF SCIENCE

at the

MASSACHUSETTS INSTITUTE OF TECHNOLOGY

June 1991 ⌊FEB 1994⌋

© Jörgen Olsson

Signature of Author _____
Deparment of Aeronautics and Astronautics
March 15, 1991

Certified by _____
Professor Mårten Landahl
Thesis Supervisor

Accepted by _____
Professor Harold Y. Wachman
Chairman, Department Graduate Committee

Localized Disturbances in a Flat Plate Boundary Layer

b y

Jörgen Olsson

Abstract

An experimental investigation of how small, localized disturbances evolves and spreads in a laminar boundary layer has been made. Two different types of disturbance generators were used. The first consisted of circular latex membranes mounted flush with the surface of a flat plate. The membranes were used in single or double configuration in order to generate the different desired disturbances. The disturbances in the flow was generated by letting the membranes deflect in or out of the wall for a short time. The second type of disturbance generator was a narrow slot of lenght comparable to the diameter of the membranes, also mounted flush with the flat plate. The slot could be rotated 360 degrees to allow for different types of disturbanes. The disturbances from this type of generator was created by sucking or blowing a short pulse of air

through the slot. The development of the disturbances downstream were mapped by traversing a hot-wire in the spanwise and normal directions to the plate at several locations downstream of the disturbance generator. At each measurement station a time record of the local streamwise velocity was taken. In this way a picture of how the disturbances evolved and spread could be conceived at different downstream locations. The aim of the experiment was to try and generate disturbances that would grow algebraically in time, Landahl [16]. The existence of this instability has been verified in direct numerical simulations of the Navier-Stokes equations for the case of plane Poiseuille flow, Henningson et. al. [20]. In the present experiment, however, this type of growth could not bedetected. Regardless of how the disturbance was generated and as long as the initial amplitude was small enough not to trigger non-linear effects, the downstream development of the disturbance had the same behaviour. One condition for the algebraic instability is that the disturbance must have a non-zero streamwise wave number zero component. The experiment was designed to satisfy this condition, especially for the case of blowing through the slot oriented parallel to the streamwise direction of the flow. A theoretical explanation for the absence of the algebraic instability in the experiment has been found. The main reason for the difference between the experiment and the numerical simulation is that the disturbance was generated at the wall instead of out in the shear layer.

Thesis Supervisor: Dr. Mårten Landahl

           Title: Professor of Aeronautics and Astronautics

Acknowledgements

I would like to thank the following people for their assistance with the work presented in this report.

Mårten Landahl, my advisor, for guiding the work and, especially for the analysis in Appendix A.

Joe Haritonidis, for whom there never exists an insoluble practical problem in experimental fluid mechanics. He gave me invaluable insight to the field of boundary layers, and how to measure them.

Dan Henningson, Pieter Schmid and Fei Li for discussions of stability and transition, and the physical aspects of these phenomena.

I also would like to thank FFA for allowing and finansing my studies at MIT.

Contents

1. Introduction

The understanding of how laminar flow becomes unstable and breaks down to turbulence is of fundamental interest in most fluid mechanics applications. One reason for this is that turbulent flow around an object produces higher drag than laminar flow. Another reason is that a turbulent flow around a body has higher heat transfer rate than laminar, which is important especially for hypersonic flows.

1.1 Linear theory

The study of stability and transition started with Osborn Reynolds famous pipe flow experiment [1]. In this experiment he found that a nondimensional parameter had a critical value by which the flow changed from a smooth ordered state into a disordered one. This parameter, nowdays called the Reynolds number, is the ratio of inertial forces to friction forces and is usually written as:

$$\text{Re} = \frac{UL}{v}$$

where U is a characteristic velocity, L a characteristic lenght and v the kinematic viscosity. Reynolds thought that an instability mechanism might be responsible for this abrupt breakdown of the flow. The first to study this idea of an instabillity mechanism was Rayleigh [2] who derived the equation for the evolution of a linear wave in an inviscid parallel shear flow. He also found that in order

for a wave to become unstable in this type of flow, the mean velocity profile has to have an inflection point, i.e. a point where the second derivative of the mean velocity profile is zero which also means that the streamwise vorticity has a extremum. This work was followed by the study of the viscous case by Orr [3] and Sommerfeld [4], who independently derived the now well known Orr-Sommerfeld equation. The solution of this equation later showed that flows without an inflection point could still become unstable at high Reynolds numbers. Tollmien [5] and Schlichting [6] investigated the case of boundary layer flows and estimated a critical Reynolds number, i.e. the Reynolds number were the flow first becomes unstable to infinitly small wave disturbances, to be between *420* and *575*.

Experimentally these theoretical results were more difficult to verify. The first successful atempt was done by Schubauer and Skramstad [7], who used a vibrating ribbon to create waves in a flat plate boundary layer. The ribbon could be made to oscillate at desired frequenzies, and the growth and development of the waves generated could be followed downstream with hot-wires. Most of the features predicted by Tollmien and Schlichting was confirmed in this experiment, including the critical Reynolds number. The reason for the success of the experiment was that for the first time, care was taken to make sure that the flow disturbances (turbulence level) was keept low.

These first theoretical and experimental research efforts dealed

with the intital growth of infinitly small two-dimensional waves. One reason for only studying two-dimensional waves was the result derived by Squire [8], who showed that two-dimensional waves will first become unstable in a parallel shear flow. He found that an infintesimal oblique wave can be transformed into an equivalent two-dimensional one at a lower effective Reynolds number.

Klebanoff, Tidstrom and Sargent [9] found in an experimental investigation, using the oscillating ribbon technique, that after the initial linear development of the waves they quickly became highly three-dimensional. This tree-dimensionality was artificially enhanced by putting small pieces of tape at regular spanwise interwalls beneath the ribbon. This produced waves having a spanwise variation. The peaks of this spanwise variation was advected faster than the valleys, and forming into lambda shaped vorticies that quickly broke down to turbulence in a series of high frequenzy spikes. Kovasznay, Komoda and Vasudeva [10] explored these lambda vorticies further, and found that they were associated with sharp internal shear layers.

1.2 Localized disturbances

Another approach to the problem of stability of shear layers is to study how a localized (in time and space) three-dimensional disturbance developes as it is advected downstream by a mean flow. This is mathematically a classical initial value problem approach. The

first to study this problem was Orr [3] who solved the linear two-dimensional initial value problem for inviscid Couette flow. He showed that in the inviscid case there must exist a continuous spectrum of modes in addition to the discrete modes governed by the Rayleigh equation in order to account for a general initial disturbance. This continuous spectrum results from the singularity in the inviscid equations which is a result of neglecting the viscous terms. The singularity occurs where the phase speed of the waves equals the local mean velocity. For viscous flows another continuous spectrum exists associated with the existence of one or more free boundaries. This can be found either by solving the Orr-Sommerfeld equation, assuming oscillatory eigenfunctions at infinity, Grosch and Salwen [11], or by using the initial value approach where it appears in a natural manner, Gustavsson [12].

Case [13] and Dikii [14] outlined a solution for a general two-dimensional parrallel flow. They showed for this case that only the discrete spectrum can cause growth since the continuous spectrum always will decay. Landahl [15], however, found by analysing the three-dimensional problem that an additional effect arises from the fact that when a fluid element is displaced vertically it still retains a major part of its horisontal momentum. The result is a contribution to the horizontal velocity if there is a mean shear present. This produces a *permanent scar* in the flow. Landahl also found [16] that this effect will cause an algebraic instability when low streamwise wave numbers are excited, which means that the energy for a disturbance having a streaky shape will grow linearely in time.

Hennigson [17] noted that the *lift-up* of a fluid element is directly proportional to the normal vorticity component.

Breuer [18] carried out an extensive investigation of the development of initial disturbances in laminar boundary layers. He made both an experimental and a numerical investigation of the problem. By using rubber membranes mounted flush with the surface of a flat plate hegenerated pulse-like disturbances in the boundary layer. For small disturbances he found that the transient portion of the disturbance decayed exponetially whereafter a wave packet, formed by the dispersive wave modes, started to develop, which was in good agreement with the theory of Gaster [19]. For high amplitudes of the disturbance (to large to be assumed infinitesimal), the shear layer created by the transient distorted the local mean profile sufficiently to allow a secondary shear-layer-type instability to grow.

Henningson, Johansson and Lundbladh [20] investigated weak initial disturbances in plane Poiseiulle flow with direct numerical simulations of the Navier-Stokes equations. They used an initial disturbance consisting of two counter-rotating vortices. When the vortices were parallel to the mean flow direction the evolution of the disturbance was shown to be associated with the spreading of a wave packet. By rotating the initial disturbance more than 10 degrees from the mean flow direction they demonstrated that the total energy of the disturbance showed linear growth in time. This, they concluded, was caused by the net lift-up effect created when the disturbance

were rotated.

1.3 Present work

The present work is an experimental investigation aimed at verifying the existence of algebraic instability in a flat plate boundary layer. The work follows Breuer [18] in much of the experimental details where, e.g., his type of disturbance generator has been mainly used. In his work, Breuer tried to simulate the symmetric type of disturbance he used in his theoretical work. Here, however, the approach is to try and generate a disturbance that resembles the rotated symmetric disturbance used by Henningson et. al. [20]. The way this has been done is to use two rubber membranes mounted flush with the surface operating together with precise timing and, with variable orientation to each other. Also thin slots of different width were used as disturbance generators, for which the orientation of the slot could be varied.

A related topic is also described in addition to the experimental work. This is an numerical investigation of the inviscid stability of the Blasius boundary layer profile.

2. Experimental setup

2.1 Wind tunnel

The experiment was carried out in the Low Turbulence Research wind tunnel (figure 1) located at MIT. The tunnel is a low-speed, fan driven, closed loop facility. The test section is 6 m long and has a cross-section area of 2 by 4 ft. The maximum velocity is around 40 m/s and the streamwise velocity turbulence fluctuation level has been measured to be less than 0.02 %. The minimum velocity, that can be used and still retain good flow conditions is about 0.5 m/s.

The tunnel has two interchangable test sections. The one used for this experiment has a 6 m long flat plate mounted vertically in the test section which has been used for fundamental flat plate studies of laminar, transitional and turbulent boundary layers. The other test section is empty exept for a traversing mechanism, and have been used for a variety of different flow experiments. The flat plate, made from aluminium, is 0.5 in thick and has an elliptical tapered leading edge. It is joined to the floor and ceiling by porous metal plates, through which suction of the boundary layers developing in the corners can be applied. In the plate there are inserted several plugs of plexiglass suitable for installing various types of measurement equipment and for makeing flow modifications. The walls parallel to the flat plate are diverging and

are adjusted to give zero pressure gradient in the test section. However, this adjustment was done for a tunnel speed of 40 m/s and does not entirely hold for the speed used in this experiment, which was 8 m/s. The effect of this is further discussed in chapter 3. The plate also has a trailing edge flap for pressure gradient adjustments.

All measurements were made using constant temperaure hot-wire anemometry. The hot-wire probes was mounted on the traverse system in the tunnel. This traverse system was computer controlled and could move the probes in all three directions. The system is controlled by a Modulynx motion control unit and traversing is done with step motors. The hot-wire probes was built inhouse, and the type mainly used in this experiment was a single wire probe with a 1.27 µm diameter Wollaston wire, with a lenght of 400 µm giving a L/D around 315 (figure 2). The anemometer amplifiers were also built inhouse and were operated at a overheat of the probes at 30%. The signal from the hot-wire was amplified and offset in order to use the maximum resolution of the analog to digital converter which was from -10 to +10 volts.

It is very important to keep the temperature of the air in the tunnel constant in order to avoid drift of the hot-wire anemometers used for the measurements. This was achieved with a heat exchanger which kept the temperature at a constant level after a stabilizing run time of ca 15 minutes.

All data were aquired using a Phoenix Data ADC (Analog to

Digital Converter) connected to a MicroVAX II computer. The maximum sampling speed of this system is 333 KHz for a single channel. The ADC can sample up to 16 channels simultaneously using a sample-and-hold circut on each channel. The MicroVAX II controlled the traversing system by using a terminal line connected to the Modulynx units RS-232 port. The computer was also used to download and program the small microcomputer of type NMIX-0022 which controlled the valves used to create the disturbances. This microcomputer was also connected via a terminal line from the MicroVAX to it's RS-232 port. Figure 3 shows a schematic of the measurement system. The way in which the microcomputer controlled the valves will be described below.

2.2 Disturbance generators

Two types of disturbance generators were used. The first was a further development of the technique used by Breuer [18] and consisted of circular membranes made of latex. The membranes (figure 4) were stretched across circular plexiglass plugs of diameters varying from 9 to 25 mm. Beneath the mebranes there was a cavity of 0.5 mm depth and with a diameter slightly less than the outer diameter of the plug. In the bottom of the plugs two holes were drilled. These holes were connected to either high or low pressures through pressure tubes. High pressure was supplied by a 250 bar pressure vessel. The pressure was regulated down to approximatively 1 bar above atmosphere. Low pressure was

supplied by a small vacuum pump. Also this pressure was regulated and was keept slightly below atmospheric pressure. The whole plug was then mounted flush with the surface of one of the larger plexiglass plugs in the flat plate. Two membranes of equal diameter were mounted side by side and the larger plug could be rotated 360 degrees. This made it possible to generate different types of disturbances dependent on at which angle the membranes were placed to each other and it also allowed for a study of different parameters that influence the structure and shape of the disturbance.

The disturbances in the flow were generated by either sucking or blowing air into the cavity beneath the membrane. This made the membrane deflect either in or out of the flat plate and thus either dragging high speed fluid closer to the wall or pushing low speed fluid away from the wall. This was done during a short time (4-10 ms) and in this way a pulse-like disturbance was created in the boundary layer.

The other type of disturbance generator consisted of thin slots mounted in small plugs (figure 5). The lenght of the slot was chosen to be comparable to the diameter of the membranes and two slot widths were used, 25 and 250 µm. The slots were constructed by placeing two pieces of thin glass parallel to each other. The pieces of glass had strait sharp edges and were glued on to the plexiglass plug using a fine spacer in order to achive the the small width. Underneath the slot a small sealed cavity was made and this had

two pressure tubes that were connected to high and low pressures, respectively.

For this case the disturbances was created by sucking or blowing a short pulse of air through the slot and in this way achieving a disturbance in the flowfield that reasembeled the ones made with the membranes. In this case, however, mass was either added or subtracted from the flow field, but this did not seem to alter the sensibility of the boundary layer to the disturbances. The slots could be rotated 360 degrees, which made it possible to vary the shape of the generated disturbances. A schematic view of how the disturbance generator and hot-wire was oriented on the flat plate is seen in figure 6.

2.3 Hot-wire calibration and measurement

The hot-wires were calibrated in the test section of the tunnel. The free stream velocity was checked by a pitot tube mounted on the traverse system. The calibration usually consisted of seven calibration points fitted to a cubic polynomial. Instead of using the polynomial to calculate the velocity during the measurements a calibration table was used. This was done by using the fact that the ADC having 12 bits resolution and used in bipolar mode gives integer values from -2048 to 2047 corresponding to voltages from -10 to +10 volts. A velocity was calculated for each of the 4096 integer values given out from the ADC and stored in an array of lenght 4096.

The measured output from the hot-wire was then used as an index in the calibration array to get the velocity. In this way the six multiplications and three additions needed to calculate the velocity from a cubic polynomial is replaced by simple indexing in an array. For this particular measurement this increase in calculation speed was not crucial since only 512 or 1024 points were measured at a time, but for turbulence measurements, where several houndreds of thousands of points are collected, this procedure can save much computer time. A simple example routine in FORTRAN is found in Appendix B. The calibration of the hot-wires was checked frequently and maximum allowed deviation was 0.5%. If the deviation was found to be more than this, but within a few per cent, the output of the anemometer was adjusted to the calibrated value by using the voltage offset. This new value was then checked over the entire calibration range and usually found to be within the desired limit. Since the tunnel was kept at constant temperature the main source of drift of the hot-wires was from temperature drift of the anemometer circuts.

2.4 Measurement arrangement

The flow field was mapped by traveresing a singel hot-wire in different x-planes downstream of the disturbance generator. In this way a time record of the streamwise velocity of the disturbance could be measured as it passed a specific x-station.

The whole experiment was controlled by the MicroVAX II

computer. The measurement program communicated with the ADC and the traversing system directly and with the microcomputer indirectly. First the probe was manually positioned at a desired starting location, usually at the centerline of the disturbance, and at a distance from the wall within the linear part of the laminar boundary layer. From this position the program moved the probe to the different measureing positions according to a predefined pattern. The distance from the wall was found by measuring the velocity at the first position and then using a linear interpolation scheme for the linear part of the boundary layer to move to the desired height.

The disturbance was generated useing a 10 μs pulse that was the output from the ADC when it was called using a time delay. The 10 μs pulse triggered the microcomputer to open and close the valves in a predifined way. The usual opening time of the valves was around 5 ms. The ADC started digitizing data after the time delay, and 512 samples were taken using a sampling speed of 3,33 KHz. The time delay was chosen acording to an estimate of the advection speed of the disturbance and varied between 1 to 200 ms. This procedure was repeated 100 times at each measuring position and the mean of these 100 time records was calculated, giving a coherent signal of the disturbance. The shape of the distubance could then be found, e.g., by plotting a contour plot of the time records at a constant y-position for several z-positions. A series of these contour plots at different x-positions showed the development in time of the disturbance.

3. Wind tunnel flow quality

Before the experiment was started a thorough investigation of the flat plate mean boundary layer was conducted. This was to ensure that well defined flow conditions were present when studying the development of the initial disturbances. The boundary layer at 78 positions were measured, at 13 x-positions, ranging from 500 mm to 3500 mm from the leading edge of the plate, in steps of 250 mm, and at 6 z-positions ; ±400 mm , ±200 mm and ±5 mm. A plot of all profiles together with the theoretical solution of the Blasius equation can be seen in figure 7. All profiles fall on top of each other. This has been accomplished by calculating a virtual origin for each profile. The non-dimensional distance from the wall is defined as

$$\eta = y\sqrt{\frac{U}{v(x-x_0)}}$$

where x_0 is the virtual origin, which is due to the fact that the plate has a blunt leading edge. Figure 8 shows how the measured displacement thickness along the centerline of the plate compares to the theoretical value for the same profiles. As can be seen the variations are less than 1 % for most x-locations. The change of the virtual origin with distance from the leading edge is shown figure 9. This increase of the virtual origin means that at each subsequent position, the boundary layer looks like it has started further downstream than the previous, and this is an indication that the flow is accelerating and thus having a adverse pressure gradient. A check of the setting of the angle of the flat plate showed that it was

installed to give zero pressure gradient at a free stream speed of 40 m/s. As the experiment described here were carried out at 8 m/s, free stream velocity, the flow was accelerated because of the thicker boundary layers developing on the walls at the lower speed. An estimate of the pressure coefficient parameter defined as [21]

$$x^* = \frac{x}{U(x)} \frac{dU}{dx}$$

gave a value of approximatively -0.01, which gives a slightly more stable boundary layer then the Blasius solution. It was considered that this slightly more stable boundary layer would not significanly alter the behaviour of a localized disturbance introduced into it.

Another problem encountered during the boundary layer measurements was that the traverse system was not completely parallel to the flat plate. When doing a traverse in the z-direction the measured velocity varied, even though the probe should have been at the same distance from the wall. A typical example is seen in figure 10 where the displacement thickness measured 1000 mm from the leading edge of the plate is compared with the mean value at this x-location. The problem was solved by at each measurement location traversing the probe in the y-direction to find the distance from the wall having the same mean velocity. The technique used to acheive this was to measure the velocity at two points within the linear part of the boundary layer, ($u/U_\infty < 0.5$), and then using a linear curve fit to these points to find the location with the desired mean velocity, after which the probe was moved to this location.

The last major problem encountered while doing the mean flow measurements was that the whole traversing system was vibrating. This vibration was clearly seen on an oscilloscope when the probe was close to the wall. In order to damp the vibrations a profiled airfoil section, made of poly-uretane, was placed over the main beam of the travesing system. This helped to some extent, but to get adequate damping, the two ends of the airfoil holding the y-traverse in the traversing system was fixed to the wall by plasticine. For measurement of mean bounday layer profiles, this procedure was used but not for the measurement of the development of the initial disturbances. The velocity fluctuations from the vibration was at least one order of magnitude smaller than the generated disturbances, for most cases, and the influence on the measured time signal were minimized through the averageing procedure used.

4. Measurements

The measurements will be presented in three parts. The first is basically a repetition of the measurements conducted by Breuer [18] in the same facility. This concerns the development of symmetric disturbances generated by a single membrane going either up-down (positive disturbance) or down-up (negative disturbance). The second part shows different configurations of membranes, mainly combinations of two membranes but also single membranes with different dampings and opening times. Finally, results will be presented from the disturbances genereted by the narrow slots. This includes both sucking and blowing through the slot and rotations of the slot, positioning it at different angles to the flow.

4.1 Positive and negative symmetric disturbances.

Figure 11a-e shows the downstream development of a positive disturbance from the 15 mm diameter membrane. The probe is placed at a specified location in the boundary layer, usually where the velocity is around 30% of the mean flow value, on the centerline behind the disturbance generator. The time axis shows the total time during which the measurement is done. This time starts after a delay corresponding to the streamwise distance between the generator and the measurement location. The non-dimensional distance from the disturbance generator is defined as

$$x / \delta^* = \frac{\left(x_{Meas} - x_{membrane}\right)}{\delta^*_{membrane}}$$

The mebrane is first pushed out of the wall by a small pulse of air in the cavity beneath the mebrane. This gives a decrease in velocity at the location of the hot-wire probe, since low speed fluid is deflected away from the wall. After ca 5 ms the valve is vented to the atmosphere. This makes the membrane go down and even overshoot a little, thus giving an increased velocity at the location of the probe. In figure 10a, this can be seen clearly. The x-location is here 25 displacement thicknesses downstream of the center of the membrane ($x / \delta^* = 25$) and the peak to peak amplitude is 2.1% of the free stream velocity. After another 15 displacement thicknesses downstream (figure 11b, note that the vertical scale is adjusted to the peak-to-peak amplitude for these plots) the positive overshoot of the velocity is almost damped out. The negative part still looks like a transient pulse but the peak-to-peak amplitude has dropped to 0.88%. At 100 δ^* downstream of the disturbance (figure 11c) the amplitude has dropped to 0.47% but the shape of the disturbance still looks similar to the one in figure 11b. A small drop in velocity can be suspected ahead of the main negative peak. In figure 11d this small drop has developed into a new wave lenght of the disturbance. The distance is 150 δ^* and the amplitude is now down to 0.37%. After this the disturbance is only spreading in x and z directions and in figure 11e ca 3.5 wave lengths can be seen. The disturbance has evolved into a wave packet. The distance is here 400 δ^* downstream of the disturbance generator. The amplitude is still ca 0.40% and it stays

almost constant at this value down to $x/\delta^* \approx 600$. Further downstream the disturbance will start to grow. A subharmonic appears, the amplitude of which will grow, whereafter non-linear effects take control and the disturbance quickly breaks down into a turbulent spot. The last scenario is outside the scope of this experiment and will not be discussed further. Figures 12a-e show how a negative disturbance develops. As can be seen, the shapes at the various x-positions look the same as for the positive disturbance but have a phase shift of 180°. The amplitude of the initial disturbance for this case is lower than for the positive disturbance, only 0.26 % at $x/\delta^* = 25$. For this particular initial amplitude the disturbance was hard to pick out from the background noise by the averaging technique. For $x/\delta^* > 50$ this is partly due to the low amplitude, only ca 0.06% corresponding to ca 5 mm/s, and partly due to the vibration of the traversing system. For these measurements a digital band-pass filter was employed to pick out the features of the signal. The disturbances at $x/\delta^* = 100,150$ and 350 are shown in figure 12c, d and e respectively, and resemble those shown in figure 11c-e except for the phase shift. This development af the disturbance are similar to what Breuer [18] found, and the wave packet spreading part, after the initial transient has decayed, agrees with the theory of Gaster [19].

The amplitudes for the two cases were nondimensionalized with its respectivly initial amplitude and plotted against non-dimensional downstream distance in figure 13a. The behaviour of the two cases are similar and agrees also with the results of Breuer [18].

In figure 13b the subsequent growth of the wave packet far downstream can be seen.

4.2 Unsymmetric disturbances

With unsymmetric disturbances is meant disturbances generated by using two membranes operating together but with predefined time lag and distance between them. The aim of this was to try and produce a disturbance that contained energy in the wave component with zero wavelength in the streamwise direction. This was done by rotating the mebranes so that a line connecting their respective centres, was at an angle to the free stream direction. A typical development of this type of disturbance is presented in figures 14a-e. In these figures the full line represents positive velocity and the dotted line negative. The initial disturbance at x/δ^* = 12 is clearly skewed (figure 14a) with one part phase shifted 180° ahead of the other. This pattern quickly becomes smeared out to one distinct, slightly skewed disturbance after a distance of only $14\ \delta^*$ further downstream (figure 14 b). At the same time the amplitude has dropped with the same rate as in figure 13a. After another 24 δ^* the symmetric wavepacket is discernible (figure 14c) and further downstream the wavepacket only grows in the x- and z-directions (figures 14d-e). Figures 15a-c shows the same scenario for a phase shifted initial disturbance with the only difference in behaviour of the disturbance downstream being a phase shift in the wave packet. It should be noted that the vertical scale of figures 14 and 15 are adjusted to the size of the disturbance. In figure 16 a schematic of

different types of initial disturbances that were tried is shown. All of these gave the same downstream development of the disturbance exept for the phase shift.

In order to show that a disturbance have energy at $\alpha = 0$, the time signal have to be converted to a space signal and then Fourier transformed. But to do this the phase velocity and also the dispersion relation of the disturbance have to be measured. This can be done, but was considered to be outside the time frame of this work. It can be said though, that the time signal contained energy at $\Omega = 0$, which implies that this is true also for the wave number.

Unsymmetric disturbances were also produced by using the thin slots to produce the disturbance. Here the non-symmetry was produced by rotating the slot to different angles to the mean flow direction. Also in this case the same type of wave packet appeared and developed in a similar way as for the membranes. The initial transient decaying where after a dispersive wave packet appears. Even for the case with the slot parallel to the flow direction no change of disturbance development could be found. This was most surpriseing since this type of disturbance basically is two streamwise vortices, whom will have most of their energy in spanwise wavenumbers at low streamwise wave numbers. An explanation for the absence of algebraic instability is given by the analysis in Appendix A.

5. Inviscid theory

5.1 Solution of the Rayleigh equation for the Blasius solution of the laminar boundary layer.

An investigation of the inviscid stability of boundary layer profiles was done in order to get a simple and fast tool to investigate profiles having an inflection point. The code that was written to this cause was used to find the full dispersion relation for a Blasius boundary layer. This result is included here as it is belived that it has not been previously published.

5.2 Equations

The Rayleigh equation can be derived from the two-dimensional unsteady Euler equations

$$u_x + v_y = 0$$
$$u_t + uu_x + vu_y = -p_x$$
$$v_t + uv_x + vv_y = -p_y \tag{5.1}$$

with the boundary conditions

$$u(0) = v(0) = u(\infty) = v(\infty) = 0$$

These equations have been derived using the following non-dimensionalisations

$$y = \frac{y^*}{\delta^*} = \frac{y^*}{1.7208\left(\frac{vx}{U_0}\right)^{\frac{1}{2}}} \quad ; \quad u = \frac{u^*}{U_0} \quad ; \quad v = \frac{v^*}{U_0} \quad ; \quad p = \frac{p^*}{\frac{1}{2}\rho U_0^2}$$

The assumptions made are that the flow is parallel, i.e. the mean flow is parallel to one of the coordinate axes. In this particular case the mean flow is taken to be in the direction of the flat plate and only dependent on the distance from the plate. Thus the velocities may be written

$$u(x,y,t) = \overline{U}(y) + u'(x,y,t)$$
$$v(x,y,t) = v'(x,y,t)$$

and the pressure is assumed to be constant

$$P(x,y,t) = \text{Constant} + p'(x,y,t)$$

Inserting this into (5.1) and neglecting terms quadratic in the disturbance quantities gives

$$u'_x + v'_y = 0$$
$$u'_t + \overline{U}u'_x + v'\overline{U}_y = -p'_x$$
$$v'_t + \overline{U}v'_x = -p'_y$$

$$(5.2)$$

The coefficients of (5.2) depend only on y, which means that the equations admits solutions which depend on x and t exponetially.

Solutions of the form

$$u' = \hat{u}\exp[i(\alpha x + \alpha ct)]$$
$$v' = \hat{v}\exp[i(\alpha x + \alpha ct)]$$
$$p' = \hat{p}\exp[i(\alpha x + \alpha ct)]$$

is substituted into (5.2). This gives

$$i\alpha\hat{u} + D\hat{v} = 0$$
$$i\alpha(\overline{U} - c)\hat{u} + \overline{U}'\hat{v} = -i\alpha\hat{p}$$
$$i\alpha(\overline{U} - c)\hat{v} = -D\hat{p} \tag{5.3}$$

where $D = d/dy$. Solve for the u-velocity and pressure and differentiating in the two first equations in (5.3), and then inserting this into the third gives

$$-\alpha^2(\overline{U} - c)\hat{v} = -\overline{U}'D\hat{v} - (\overline{U} - c)D^2\hat{v} + \overline{U}''\hat{v} + \overline{U}'D\hat{v}$$

which rewritten becomes the Rayleigh equation

$$D^2\hat{v} - \left(\frac{\overline{U}''}{(\overline{U} - c)} + \alpha^2\right)\hat{v} = 0 \tag{5.4}$$

The boundary conditions are

$$\hat{v}(y = 0) = \hat{v}(y = \infty) = 0$$

This equation with boundary conditions is an ordinary second order

differential equation with a regular singular point at $U=c$ and can in principle be solved analytically using Frobenius method. However, in a practical case this requires that the velocity profile has a simple analytical form. Here the Rayleigh equation is solved for the Blasius profile, which in itself comes from numerical integration of the Blasius equation and therefore a numerical approach hes been chosen. The only difficuly with the integration of the Rayleigh equation comes from the singularity and this must be treated properly. Lin [22] showed that for the solution of the Rayleigh equation to be the asymptotic solution to the viscous case as the Reynolds number goes to infinity, the integration path has to be above the real axis if $U'(ycrit)<0$ and below if $U'(ycrit)>0$, where $ycrit=y$ at $U=c$.

5.3 Numerical solution

The Rayleigh equation is easily solved by using the shooting metod. In this case the equation is written

$$(U - c)(D^2 - \alpha^2)v - U''v = 0 \qquad (5.5)$$

This is rewritten on matrix form by letting

$$\Theta_1 = v$$
$$\Theta_2 = v'$$

and becomes

$$\begin{bmatrix} \Theta_1' \\ \Theta_2' \end{bmatrix} = \begin{bmatrix} 0 & 1 \\ a & 0 \end{bmatrix} \begin{bmatrix} \Theta_1 \\ \Theta_2 \end{bmatrix} \quad ; \qquad a = \frac{U''}{(U-c)} + \alpha$$

(5.6)

This equation system is solved by using a 4th order Runge-Kutta scheme. The boundary conditions are given from vertical velocity vanishing on the wall and at infinity. The metod of solution is to first define a integration path in the complex plane going around the singularity at $U=c$. Since the derivative of a Blasius profile is everywhere positive the integration path has to lie on the negative side of the real axis. Figure 17 shows the integration path used for the calculations presented here. A Blasius profile is also included as reference. It can be seen that the path is in the complex plane from the wall and up to where the derivative of the velocity vanishes. This is necessary for these specific calculations since the wave number range used gives phase speeds of order unity. The next step is to solve the Blasius equation using the chosen integration path. This is done by using the shooting method and a 4th order Runge-Kutta scheme. The integration is here from the wall out to where the velocity is one. A complex form of the equation has to be used since the integration path is complex. The second derivative of the velocity has to be calculated. Then the Rayleigh equation is solved using the velocity profile and second derivative from the Blasius solution as coefficients. Care has to be taken to scale the second derivative in the right way. The Blasius equation is non-dimensionalized with the length

$$l_B = \left(\frac{2\nu x}{U_0}\right)^{\frac{1}{2}}$$

and the Rayleigh equation with

$$l_R = \delta^* = 1.7208\left(\frac{\nu x}{U_0}\right)^{\frac{1}{2}}$$

this gives that the second derivative of the Blasius equation has to be scaled with a factor

$$\left(\frac{1.7208}{\sqrt{2}}\right)^2 = 1.4806$$

The integration in this case is from the outer boundary (infinity) in to the wall where the condition of vanishing normal velocity has to be matched. A wave number is chosen and an initial eigenvalue, c, has to be guessed. If the guess is sufficiently close to the actual value the eigenvalue will be found. In this case the secant method is used to search for the eigenvalue that gives the right boundary condition at the wall. In practice the integration starts from a high value of y. Usually a value of y/δ^* above 6 is sufficient. Here the starting value comes from the solution of the equation at infinity where the velocity is constant and the second derivative is zero. The eigenfunctions will be of the form

$$v(\infty) = const \cdot e^{-\alpha y}$$

and the starting solution is set to

$$\tilde{\Theta} = \begin{bmatrix} e^{-\alpha y_{max}} \\ -\alpha e^{-\alpha y_{max}} \end{bmatrix}$$

A FORTRAN program that solves the Rayleigh equation has been written to calculate the inviscid stability characteristics of the Blasius boundary layer profile. The program is listed in appendix C. The eigenvalues has been calculated for $\alpha = 0.02$ to $\alpha = 2.04$. The highest value of α is restricted by the maximum phase speed. For higher α's the equation has no physical solution. The result of the calculation is shown in figure 18a-c. As can be seen the inviscid stability of the Blasius boundary layer increases for increasing wave number, which means that the Blasius boundary layer is inviscidly stable for all wave numbers. The results show good agrement with the sparse result from White [23] and Mack [24].

6. Discussion

This investigation, aimed at the study of the algebraic instability of the Blasius boundary layer, has not been able show linear growth of localized disturbances generated at the wall. The reason for this is explained in appendix A. The results of using various types of different disturbances gave no difference in the scenario of the development of the disturbance. Good agrement with the results of Breuer [18] and Gasters [19] theoretical result was achieved for all types of disturbances. The only influence found on the development of the disturbance from the shape of the initial disturbance was the phase shift. A 180° phase shift gave a 180° phase shift in the dispersive wave packet downstream.

The inviscid stability of the Blasius boundary layer has been calculated for the span of wave numbers from 0.02 to 2.04. The results agrees with what is available in the literature.

7. References

[1]   Reynolds, O. 1883. On the experimental investigation of the circumstances which determine whether the motion of water shall be direct or sinuous, and the law of resistance in parallel channels. *Phil. Trans. Roy. Soc. Lond.* 1 7 4, 935-982.

[2]   Lord Rayleigh, 1887. On the stability of certain fluid motions. *Proc. Math. Soc. Lond.* 1 1, 57-70.

[3]   Orr, W. M. F. 1907. The stability of the steady motions of a perfect liquid and of a viscous liquid. Part I: A perfect liquid; Part II: A viscous liquid. *Proc. Roy. Irish. Acad.* 2 7, 9-108.

[4]   Sommerfeld, A. 1908. Ein beitrag zur hydrodynamischen erklarung der turbulenten flussigkeitsbewegungen. In *Atti. del 4. Congr. Internat. dei. Mat. III,* Roma, 116-124.

[5]   Tollmien, W. 1931. Uber die entstehung der turbulenz. *1. Nachr. Ges. Wiss. Göttingen, Math. Phys. Klasse, Fachgruppe,* 21-44.

[6]   Schlichting, H. 1933. Berechnung der anfachung kleiner störungen bei der plattenströmung. *ZAMM* 1 3, 171-174.

[7]   Schubauer, G.B. and Skramstad, H.K. 1947. Laminar boundary layer oscillations and stability of laminar flows. *J. Aero. Sci.* 1 4, 69-78

[8]   Squire, H. B. 1933. On the stability of three-dimensional distribution of viscous fluid between parallel walls. *Proc. Roy. Soc Lond. A* 1 4 2, 621-628.

[9]   Klebanoff, P. S., Tidstrom, K. D. and Sargent, L. M. 1962. The three-dimensional nature of boundary layer transition. *J. Fluid Mech.* 1 2, 1-34.

[10]   Kovasznay, L. S. G., Komoda, H. and Vasudeva, B. R. 1962. Detailed flow field in transition. In *Proceedings of the 1962 heat transfer and fluid mechanics institute, Univ of Washington,* 1-26.

[11]   Grosch, G. E. Salwen, H., 1978. The continuous spectrum of the Orr-Sommerfeld equation. Part 1. The spectrum and the eigenfunctions. *J. Fluid Mech.* 8 7, 33-54.

[12]   Gustavsson L. H., 1979. Initial value problem for boundary layer flows. *Phys. Fluids.* 2 2, 1602-1605.

[13]   Case, K. M., 1960. Stability of inviscid plane Couette flow. *Phys. Fluids.* 3, 143-148.

[14] Dikii, L. A., 1960. The stability of plane parallel flows of an ideal fluid. *Sov. Phys. Doc.* 1 3 5, 1179-1182.

[15] Landahl, M. T., 1975. Wave break down and turbulence. *SIAM J. Appl. Math.* 2 8, 735-756

[16] Landahl, M.T., 1980. A note on an algebraic instability of inviscid parallel shear flows. *J. fluid. Mech.* 9 8, 243-251.

[17] Henningson, D. S., 1988. The inviscid initial value problem for a piecewise linear mean flow. *Stud. Appl. Math.* 7 8, 31-56.

[18] Breuer, K. S., 1988. *The development of a localized Disturbance in a boundary layer.* FDRL Report No. 88-1, Dept. Aero. & Astro., MIT, PHd thesis.

[19] Gaster, M., 1975. A theoretical model of a wave packet in the boundary layer on a flat plate. *Proc. Roy. Soc. Lond. A.* 3 4 7, 271-289.

[20] Henningson, D. S., Johansson, A. V. and Lundbladh, A. 1989. On the evolution of localized disturbances in laminar shear flows. From IUTAM, *Third symposium on laminar-turbulent transition*, Toulouse, Sept 11-15 1989.

[21] Schlichting, H. 1979. *Boundary layer theory*. McGraw-Hill, 7 ed.

[22] Lin, C. C., 1955. *Theory of hydrodynamic stability*. Cambridge Univ. Press.

[23] White, F. M., 1974. *Viscous flow*. McGraw Hill.

[24] Mack, L. M., 1976. A numerical study of the temporal eigenvalue spectrum of the Blasius boundary layer. *J. Fluid. Mech.* 7 3, 497-520.

Appendix A

Inviscid linear perturbation due to wall motion

The linearized equation for the vertical inviscid perturbation velocity reads

$$\frac{D\Phi}{Dt} - U'' \frac{\partial v}{\partial x} = 0 \qquad (A.1)$$

where

$$\Phi = \nabla^2 v \qquad (A.2)$$

with boundary conditions:

$$v(x,0,z,t) = \frac{\partial \eta}{\partial t} = v_w(x,z,t) \qquad (A.3)$$

$$v(x,\infty,z,t) = 0 \qquad (A.4)$$

where $y=\eta(x,z,t)$ describes the motion of the flexible membrane. The integration of (A.1) with respect to time gives

$$\Phi = \Phi_0(\xi,y,z) + U''l_x \qquad (A.5)$$

where subscript zero denotes initial values, $(t=0)$, and l is the fluid element liftup,

$$l(x,y,z,t) = \int_0^t v(x_1,y,z,t_1)dt_1 \qquad (A.6)$$

and where

$$x_1 = x - U(t - t_1) \qquad (A.7)$$

The membrane motion is confined to a finite time $t \le T$ after which $v_w = 0$ Solution of (A.2) with (A.5) yields

$$v = -\frac{1}{4\pi} \int\int\limits_{-\infty}^{\infty} dx_1 dz_1 \int\limits_{0}^{\infty} dy_1 U'' l_x(x_1, y_1, z_1, t)\left[\frac{1}{R_1} - \frac{1}{\overline{R}_1}\right]$$

$$+ \frac{y}{4\pi} \int\int\limits_{-\infty}^{\infty} dx_1 dz_1 \frac{v_w(x_1, z_1, t)}{\mathcal{R}^3}$$

(A.8)

where

$$R_1 = \sqrt{(x-x_1)^2 + (y-y_1)^2 + (z-z_1)^2}$$

$$\overline{R}_1 = \sqrt{(x-x_1)^2 + (y+y_1)^2 + (z-z_1)^2}$$

$$\mathcal{R} = \sqrt{(x-x_1)^2 + y^2 + (z-z_1)^2}$$

On the assumption that the fluid element liftup, l, is nonzero only within a finite range of x such that

$$l \to 0 \quad \text{for} \quad |x| \to \infty$$

(A.9)

one finds that

$$\overline{v} \equiv \int\limits_{-\infty}^{\infty} v dx = \frac{1}{2\pi} \int\int\limits_{-\infty}^{\infty} \frac{y\overline{v}_w(z_1, t)}{y^2 + (z-z_1)^2} dz_1$$

(A.10)

For $t > T$, for which $v_w = 0$, then

$$\overline{v} = 0$$

(A.11)

showing that algebraic instability cannot be generated by small amplitude wall motion in the manner tried in the experiment.

Appendix B

Example of using calibration table to find measured velocities

```
      PROGRAM TABLEX
C
      REAL*4 TABLE(-2048:2047),VELO(1024),A(4)
      INTEGER*2 INDATA(1024),TSAMP,TDELAY
C
C     READ POLYNOMIAL COEFFICIENTS FROM CALIBRATION FILE
C
      READ(1)(A(I),I=1,4)
C
C     CALCULATED VELOCITIES FOR EACH INTEGER VALUE OF THE ADC
C
      DO I = -2048,2047
           TABLE(I) = A(1) + A(2)*I + A(3)*I*I + A(4)*I*I*I
      ENDDO
C
C     COLLECT DATA FROM ADC  (ONLY EXAMPLE CALL)
C
      CALL ADC(INDATA,1024,TSAMP,TDELAY)
C
C     CALCULATE VELOCITIES
C
      DO J = 1, 1024
           VELO(J) = TABLE(INDATA(J))
      ENDDO
C
      STOP
      END
```

Appendix C

Program solving the Rayleigh equation for the Blasius boundary layer

```
        PROGRAM BLARAY
C
C==================================================================
C
C       Program that solves the Rayleigh equation for a
C       boundary layer profile.(SINGLE PRECISION VERSION)
C
C       Solves for the Blasius equation in complex form.
C
C==================================================================
C
        IMPLICIT NONE
C
        COMPLEX*8 FI1(100),FI2(100),ALFA(100),C(100),C1,C2,TEMP
        COMPLEX*8 U(199),Y(199),U2(199),D,D1,AC,BC,U2A,UA,UNEW
        COMPLEX*8 UP(199),UPNEW,UPOLD,UOLD,F(199)
C
        INTEGER NSTEP,I,J,IT,IALFA,NCIRC,NSTEP2
        INTEGER NALFA,NCIRC2,INDEX
C
        REAL*4 YMAX,AR,CR,CI,YCR,YCI,AM,ERR,RESIDUE
        REAL*4 YR,YI,THETA,PI,DALFA
C
        PI = 4.*ATAN(1.)
        ERR = 1.E-4
        YCR = 1.35
        YCI = 1.35
        NSTEP = 100
C
        YMAX = 8.0
C
C       Inital guess for eigenvalue c and alpha range.
C
        CR = 0.01
        CI = -0.01
C
        C1 = CMPLX(CR,CI)
        C2 = (0.01,0.01) + C1
C
        AR = 0.02
        AM = 2.06
```

```fortran
      NALFA = 100
      ALFA(1) = CMPLX(AR,0.0)
      DALFA = (AM-AR)/NALFA
C
C     Defining integration path.
C
      NSTEP2 = 2*NSTEP-1
      NCIRC = NSTEP/2
      NCIRC2 = 2*NCIRC+1
C
      DO I = 1,NCIRC2
         THETA = PI*(I-1.)/(NCIRC2-1.)
         YR = YCR*(1.0-COS(THETA))
         YI = -YCI*SIN(THETA)
         Y(I) = CMPLX(YR,YI)
      ENDDO
C
      DO I = NCIRC2,NSTEP2
         YR = YCR*2. + YMAX*(I-NCIRC2)/(NSTEP2-NCIRC2)
         Y(I) = CMPLX(YR,0.0)
      ENDDO
C
C     Solving the Blasius equation.
C
      U(1) = 0.0
      UP(1) = 1.660287
      U2(1) = 0.0
      CALL CBLASIUS(NSTEP2,Y,F,U,UP,U2)
      UPNEW = UP(1)
      UNEW = U(NSTEP2)
C
      UP(1) = 1.05*UP(1)
      CALL CBLASIUS(NSTEP2,Y,F,U,UP,U2)
      UPOLD = UP(1)
      UOLD = U(NSTEP2)
C
      RESIDUE = 1.E30
C
      DO WHILE(RESIDUE.GT.ERR)
         UP(1) = UPNEW-(UNEW-1.0)*(UPOLD-UPNEW)/(UOLD-UNEW)
         CALL CBLASIUS(NSTEP2,Y,F,U,UP,U2)
         UOLD = UNEW
         UPOLD = UPNEW
         UNEW = U(NSTEP2)
         UPNEW = UP(1)
         RESIDUE = ABS(U(NSTEP2)-1.0)
      ENDDO
C
C     Switching order of the elements in integration path,
C     velocity and second derivative.
```

```
C
      DO I = 1,NSTEP
         INDEX = NSTEP2+1-I
C
         TEMP = Y(I)
         Y(I) = Y(INDEX)
         Y(INDEX) = TEMP
C
         TEMP = U(I)
         U(I) = U(INDEX)
         U(INDEX) = TEMP
C
         TEMP = UP(I)
         UP(I) = UP(INDEX)
         UP(INDEX) = TEMP
C
         TEMP = U2(I)
         U2(I) = U2(INDEX)
         U2(INDEX) = TEMP
      ENDDO
C
C     Start of alfa loop !!!
C
      DO IALFA = 1,NALFA
C
C     Start integration. Integrate for each of intially
C     guessed c's and then check with the secant method which
C     way to go in order to satisfy the centerline boundary
C     condition.
C
      C(IALFA) = C1
C
C     Zero the iteration counter.
C
      IT = 0
C
C     Here starts the iteration loop.
C
 50   CONTINUE
C
C     Set up start condition. The disturbance is assumed to
C     vanish at infinity which gives the condition :
C
C     V(Y=LARGE)=EXP(-ALFA(IALFA)*Y)
C
C     This condition and its derivative is used as start
C     values for the integration.
C
      FI1(1) = CEXP(-ALFA(IALFA)*YMAX)
      FI2(1) = -ALFA(IALFA)*FI1(1)
C
```

```
C      Integration.
C
       CALL RUNGE(FI1,FI2,Y,U,U2,C(IALFA),ALFA(IALFA),NSTEP)
C
C      End of integration.
C
C      Normalize solution.
C
       DO I = 1,NSTEP
          FI1(I) = FI1(I)/FI2(NSTEP)
          FI2(I) = FI2(I)/FI2(NSTEP)
       ENDDO
       D = FI1(NSTEP)
C
C      Check determinant (here only one element) and see if
C      boundary conditon at the wall is satisfied. If not
C      calculate new c using the secant method.
C
       IF(CABS(D).LT.ERR) GOTO 100
       IF(IT.GT.2)THEN
          IF(CABS(C(IALFA)-C1).LT.1.E-6) GOTO 100
       ENDIF
C
       IT = IT + 1
       IF(IT.GT.50) THEN
         WRITE(*,*)' Number of iterations exeeded 50'
         GOTO 2
       ENDIF
C
C      First iteration proceed with second guessed c2.
C
       IF(IT.EQ.1)THEN
          C(IALFA) = C2
          D1 = D
       ELSE
          C2 = C(IALFA)-D*(C1-C(IALFA))/(D1-D)
          C1 = C(IALFA)
          C(IALFA) = C2
          D1 = D
       ENDIF
C
       WRITE(*,99)IALFA,IT,C(IALFA),D1
C
       GOTO 50
C
 100   CONTINUE
C
       C2 = C(IALFA)
       IF(IALFA.NE.NALFA) ALFA(IALFA+1) = ALFA(IALFA)
       &                                  + CMPLX(DALFA,0.0)
C
```

```fortran
      ENDDO! IALFA
C
 99   FORMAT(1X,' IALFA = ',I3,' IT = ',I2,'  C =',2F10.6,
     &             '  D =',2E10.2)
C
 2    STOP
      END
C
C================================================================
C
      SUBROUTINE RUNGE(FI1,FI2,Y,U,U2,C,ALFA,NSTEP)
C
C================================================================
C
C     Subroutine that integrates a 2D vector using a
C     fourth-order Runge-Kutta scheme.
C
C================================================================
C
      IMPLICIT NONE
C
      INTEGER I,J,NSTEP
C
      COMPLEX*8 FI1(NSTEP),FI2(NSTEP),H,A11,A12,A22
      COMPLEX*8 A21,A31,A32,A41,A42,Y(2*NSTEP-1)
      COMPLEX*8 C,ALFA,A,ALFA2,U(2*NSTEP-1),U2(2*NSTEP-1)
C
      ALFA2 = ALFA*ALFA
C
      DO I = 1,2*NSTEP-3,2
C
         H = Y(I+2)-Y(I)
         J = (I+1)/2
C
         A11 = FI2(J)*H
         A12 = (U2(I)/(U(I)-C)+ALFA2)*FI1(J)*H
         A21 = (FI2(J)+A12/2.0)*H
         A22 = (FI1(J)+A11/2.0)*(U2(I+1)/(U(I+1)-C)+ALFA2)*H
         A31 = (FI2(J)+A22/2.0)*H
         A32 = (FI1(J)+A21/2.0)*(U2(I+1)/(U(I+1)-C)+ALFA2)*H
         A41 = (FI2(J)+A32)*H
         A42 = (FI1(J)+A31)*(U2(I+2)/(U(I+2)-C)+ALFA2)*H
C
         FI1(J+1) = FI1(J)+(A11+A21*2.0+A31*2.0+A41)/6.0
         FI2(J+1) = FI2(J)+(A12+A22*2.0+A32*2.0+A42)/6.0
C
      ENDDO
C
      RETURN
      END
C
```

```fortran
C===================================================================
C
          SUBROUTINE CBLASIUS(NINT,Y,F,U,UP,UPP)
C
C===================================================================
C
C      Integrates the complex Blasius equation.
C
       IMPLICIT NONE
C
       INTEGER NINT,I
C
       COMPLEX*8 F(NINT),U(NINT),UP(NINT),UPP(NINT),Y(NINT),H
       COMPLEX*8 A11,A12,A13,A14,A21,A22,A23,A24,A31,A32,A33
                COMPLEX*8 A34,A41,A42,A43,A44
C
       DO I = 1,NINT-1
          H = Y(I+1)-Y(I)
C
          A11 = H*U(I)
          A13 = H*UPP(I)
          A14 = -H*1.4806*(F(I)*UPP(I)+U(I)*UP(I))
C
          A21 = H*(U(I)+0.5*A12)
          A22 = H*(UP(I)+0.5*A13)
          A23 = H*(UPP(I)+0.5*A14)
          A24 = -H*1.4806*((F(I)+0.5*A11)*(UPP(I)+0.5*A14)+
     &          (U(I)+0.5*A12)*(UP(I)+0.5*A13))
C
          A31 = H*(U(I)+0.5*A22)          .
          A32 = H*(UP(I)+0.5*A23)
          A33 = H*(UPP(I)+0.5*A24)
          A34 = -H*1.4806*((F(I)+0.5*A21)*(UPP(I)+0.5*A24) +
     &          (U(I)+0.5*A22)*(UP(I)+0.5*A23))
C
          A41 = H*(U(I)+A32)
          A42 = H*(UP(I)+A33)
          A43 = H*(UPP(I)+A34)
          A44 = -H*1.4806*((F(I)+A31)*(UPP(I)+A34) +
     &          (U(I)+A32)*(UP(I)+A33))
C
          F(I+1)   = F(I)+(A11+2.0*A21+2.0*A31+A41)/6.0
          U(I+1)   = U(I)+(A12+2.0*A22+2.0*A32+A42)/6.0
          UP(I+1)  = UP(I)+(A13+2.0*A23+2.0*A33+A43)/6.0
          UPP(I+1) = UPP(I)+(A14+2.0*A24+2.0*A34+A44)/6.0
C
       ENDDO
C
       RETURN
       END
```

Plan view

Cooling
Coils

Fan &
Motor

Turning
vanes

Screen &
Honeycomb

Contraction

Test
section

Diffuser

Side view
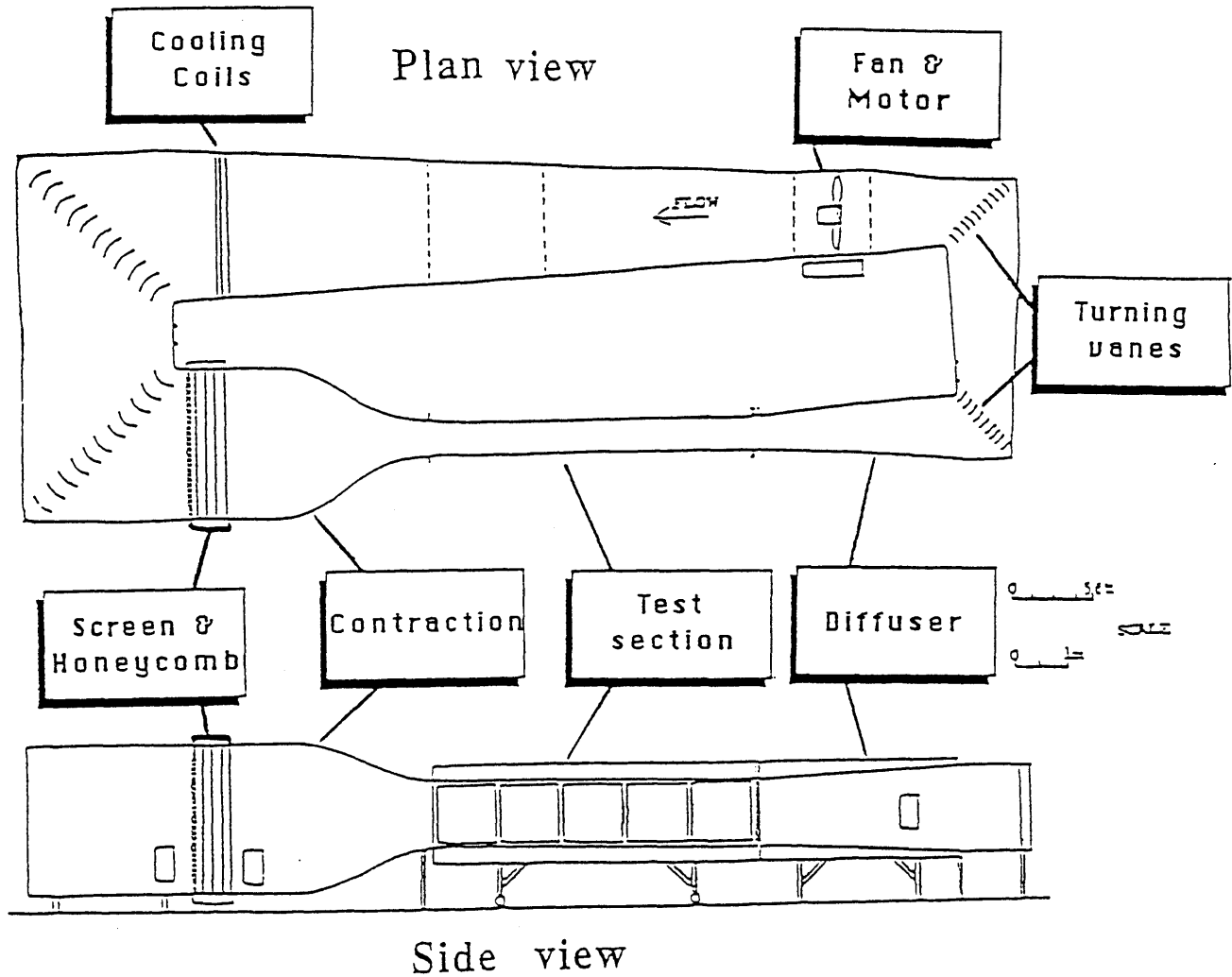
Figure 1. The low turbulence wind tunnel.

0.4
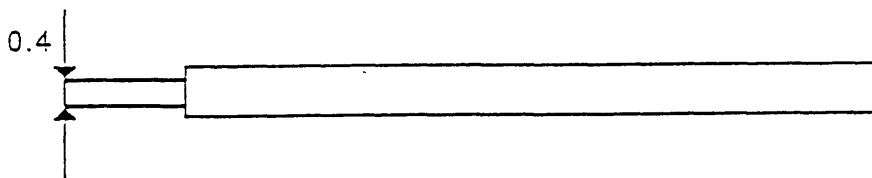
Figure 2. Hot-wire probe.
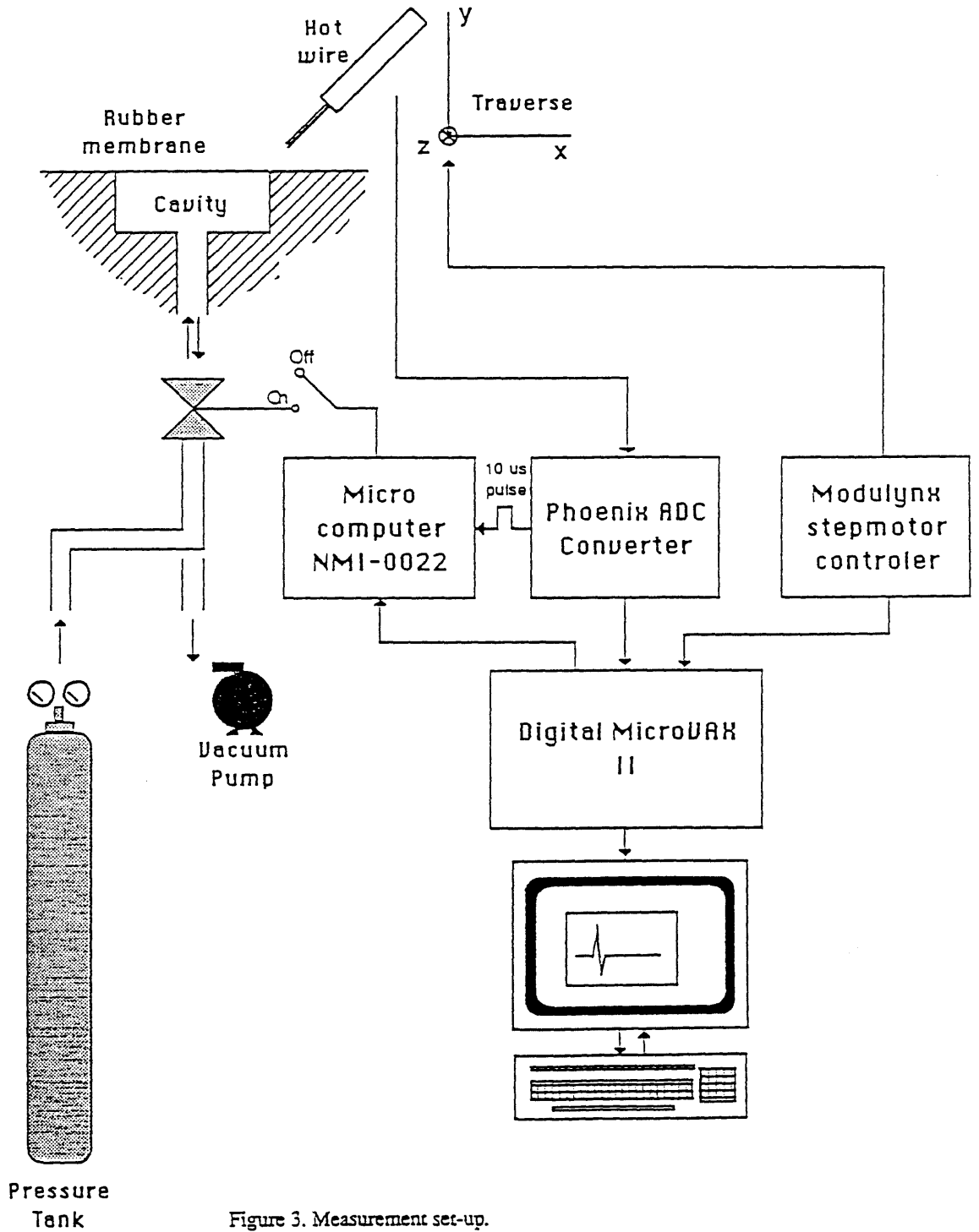
Figure 3. Measurement set-up.
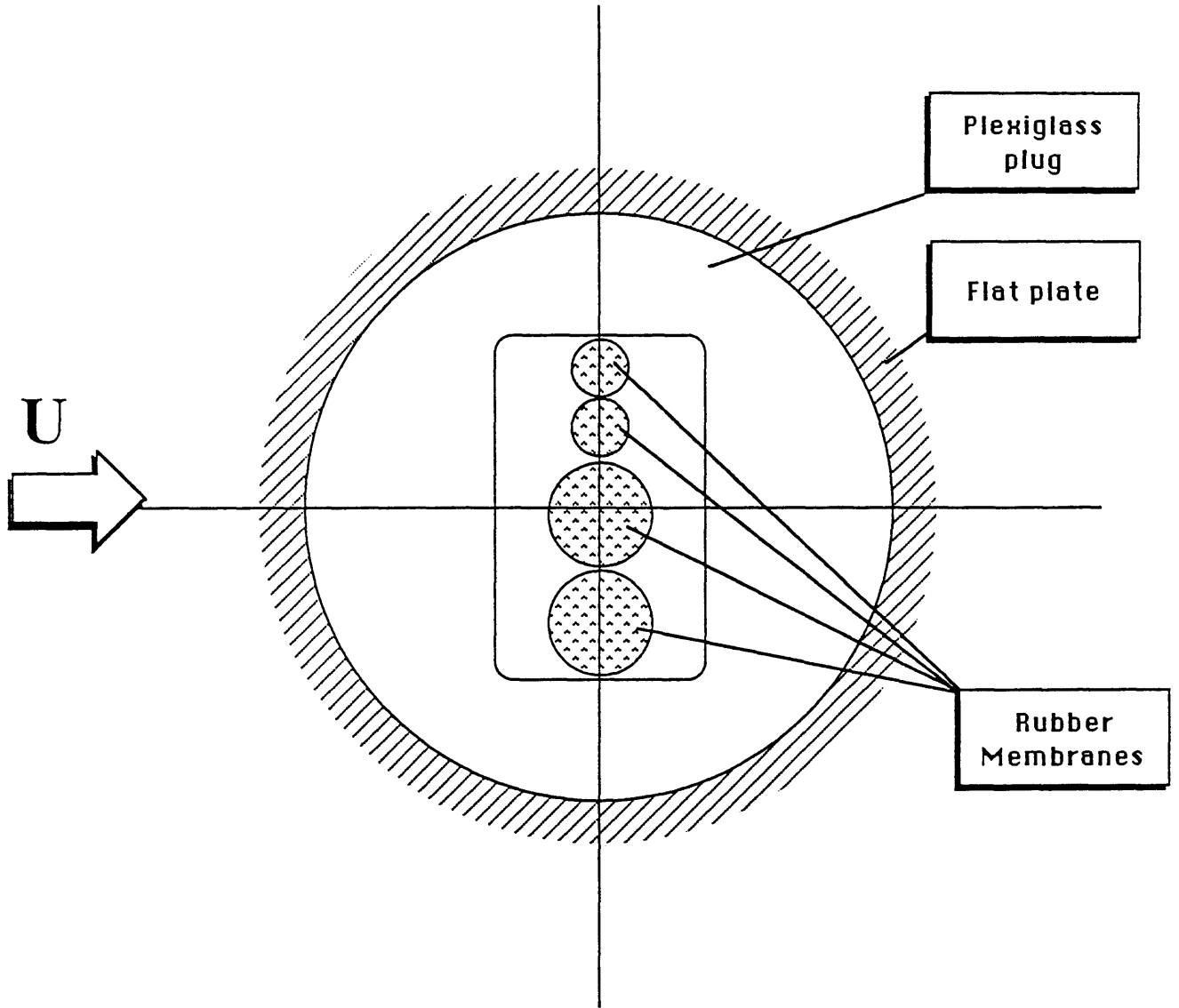
Figure 4. Membranes placed in plexiglass plug in the flat plate.
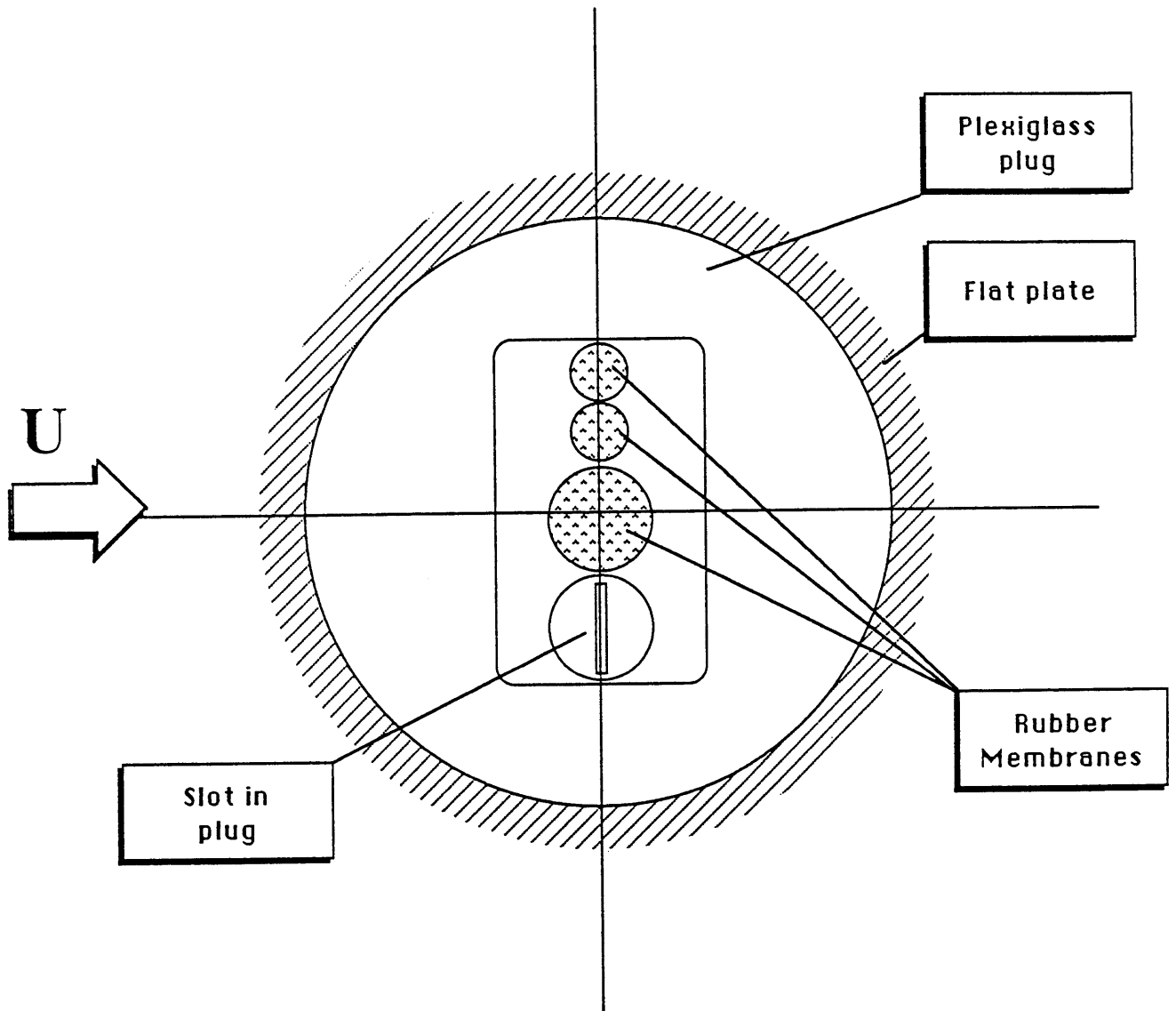
Figure 5. Plexiglass plug with slot in the flat plate.
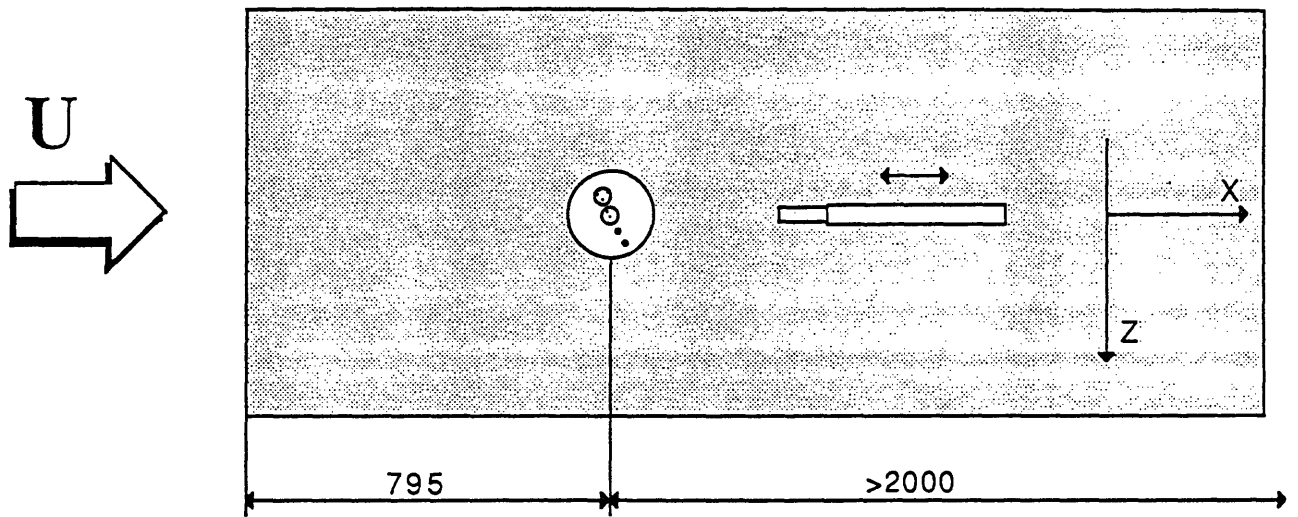
Figure 6. Location of membranes in plug in the flat plate.

$$\eta = y \sqrt{\frac{U}{v(x - x_0)}}$$
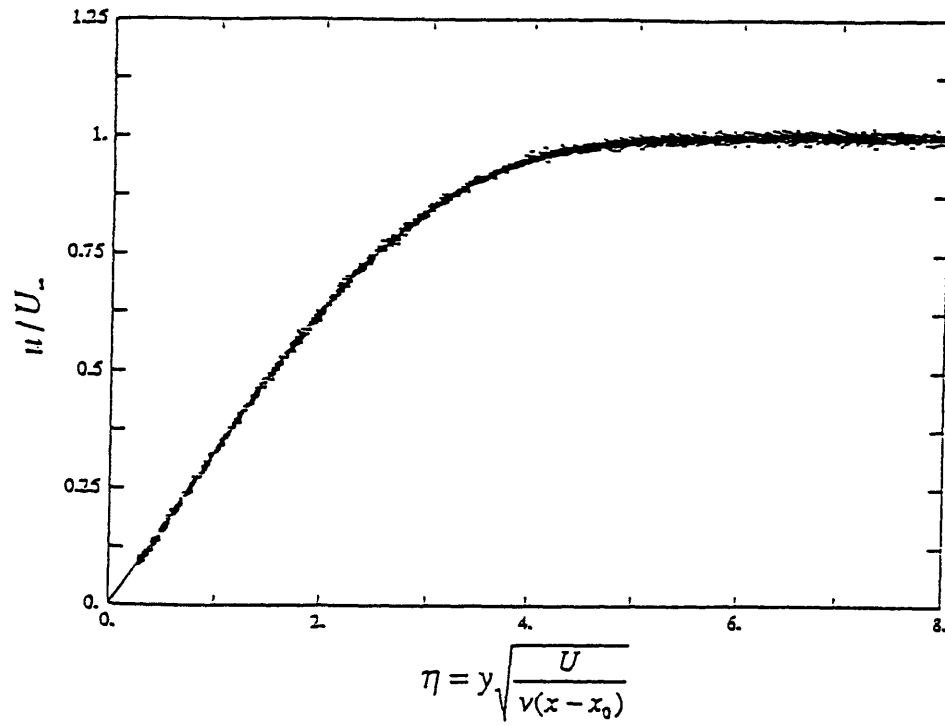
Figure 7. Mean boundary layer profiles at 78 different locations.
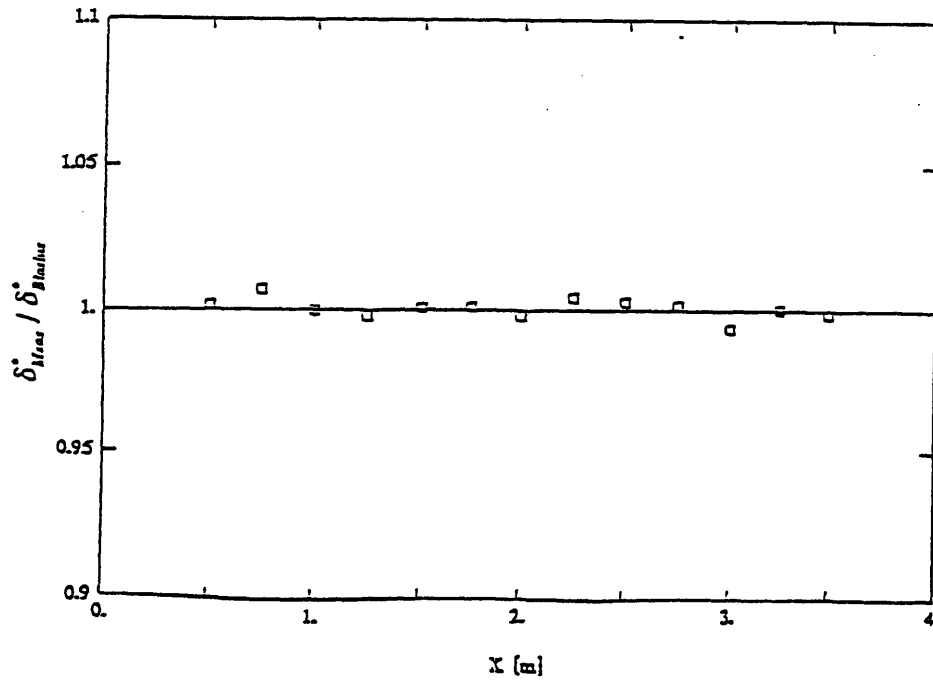
Figure 8. Measured displacement thickness deviation from the theoretical value along the centerline of the plate.
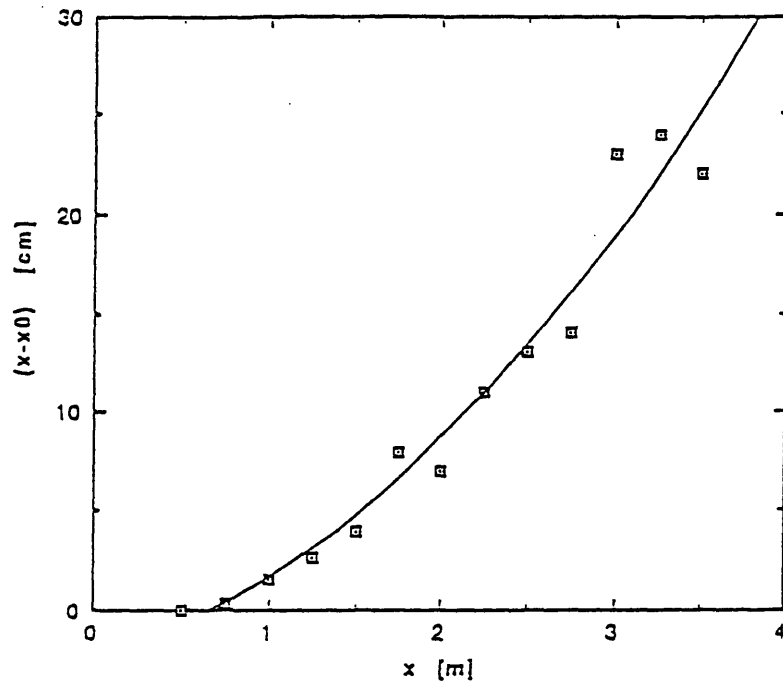
Figure 9. The virtual origin as function of distance from the leading edge. The curve is fitted to data.
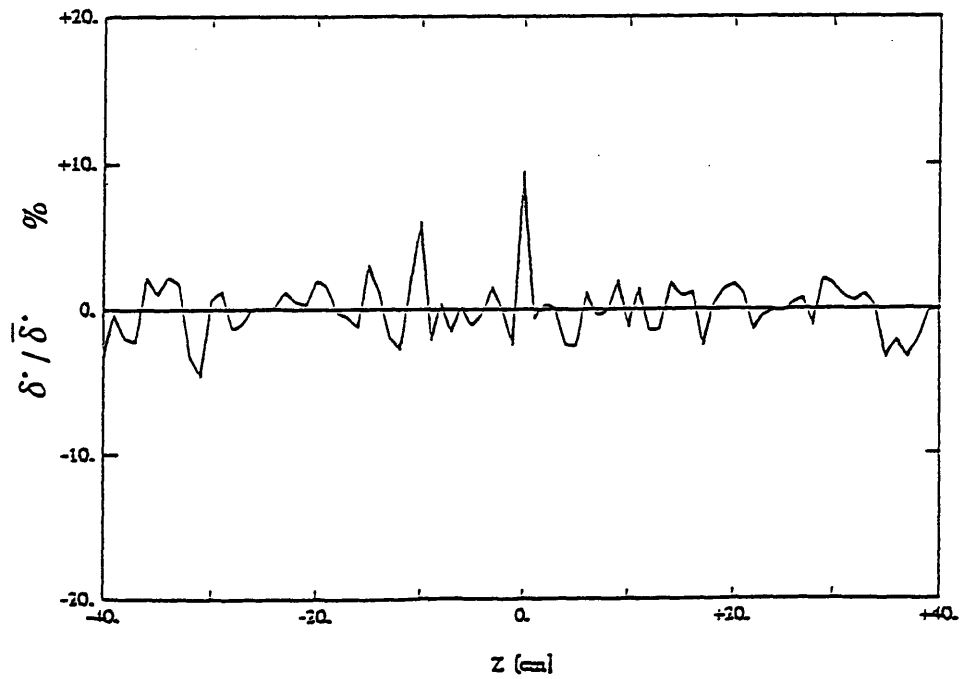
Figure 10. Variation of measured   displacement thickness in spanwise direction at $x = 1000$ mm.
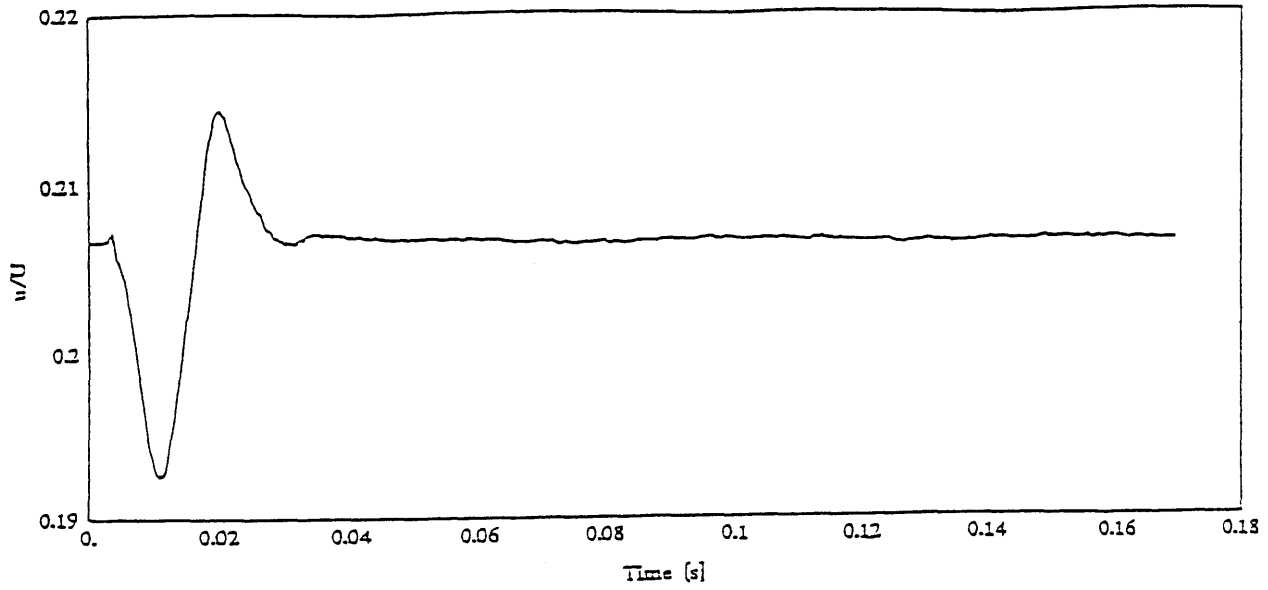
Figure 11 a. Positive disturbance. $x / \delta^* = 25$
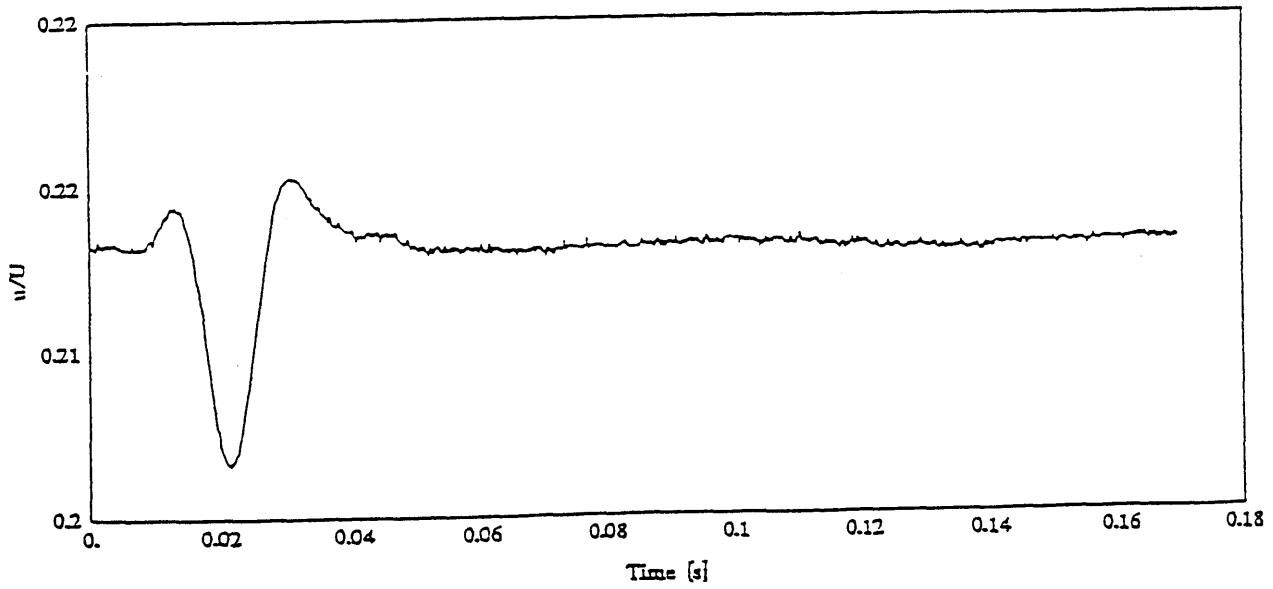
Figure 11 b. Positive disturbance. $x / \delta^* = 40$
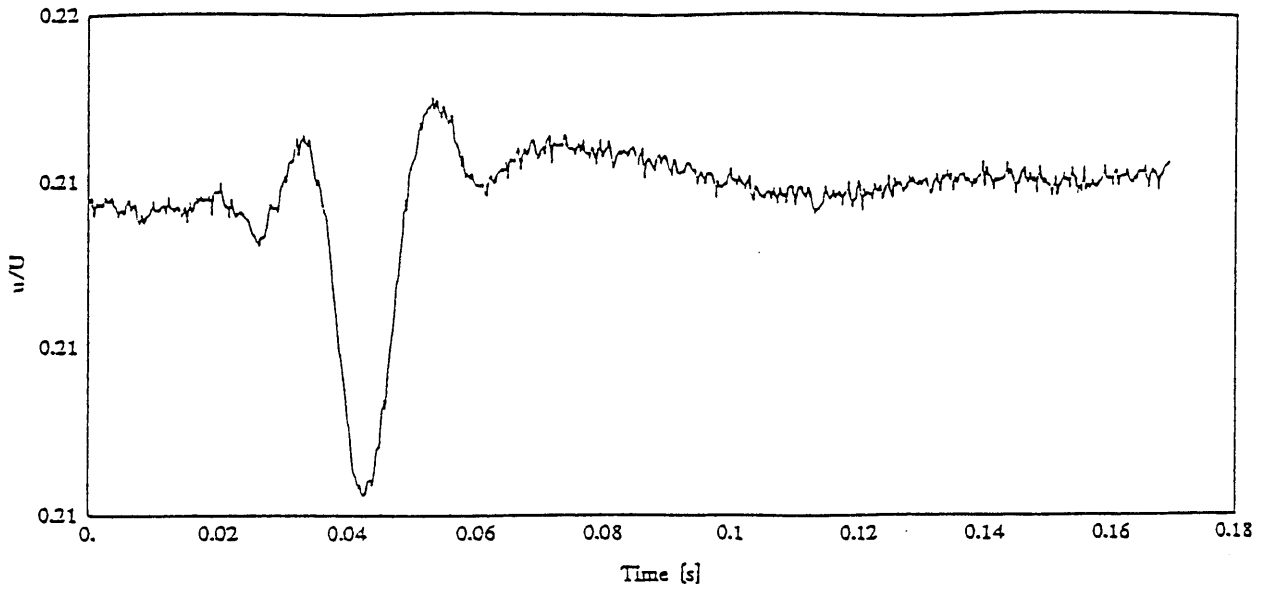
Figure 11 c. Positive disturbance. $x / \delta^* = 97$
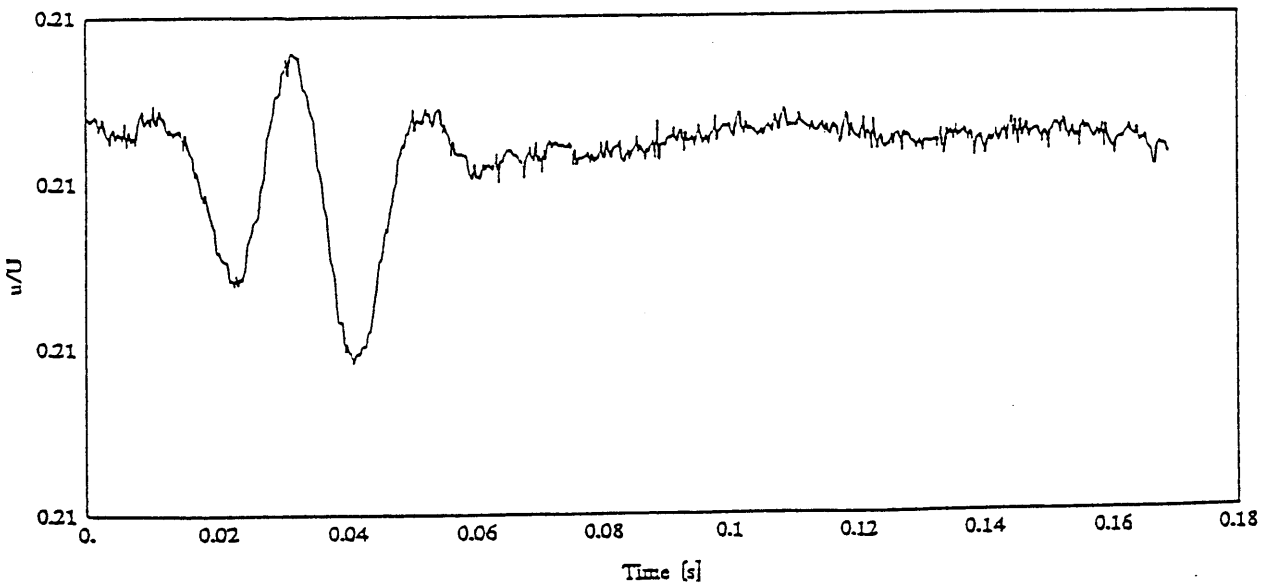
Figure 11 d. Positive disturbance. $x / \delta^* = 150$
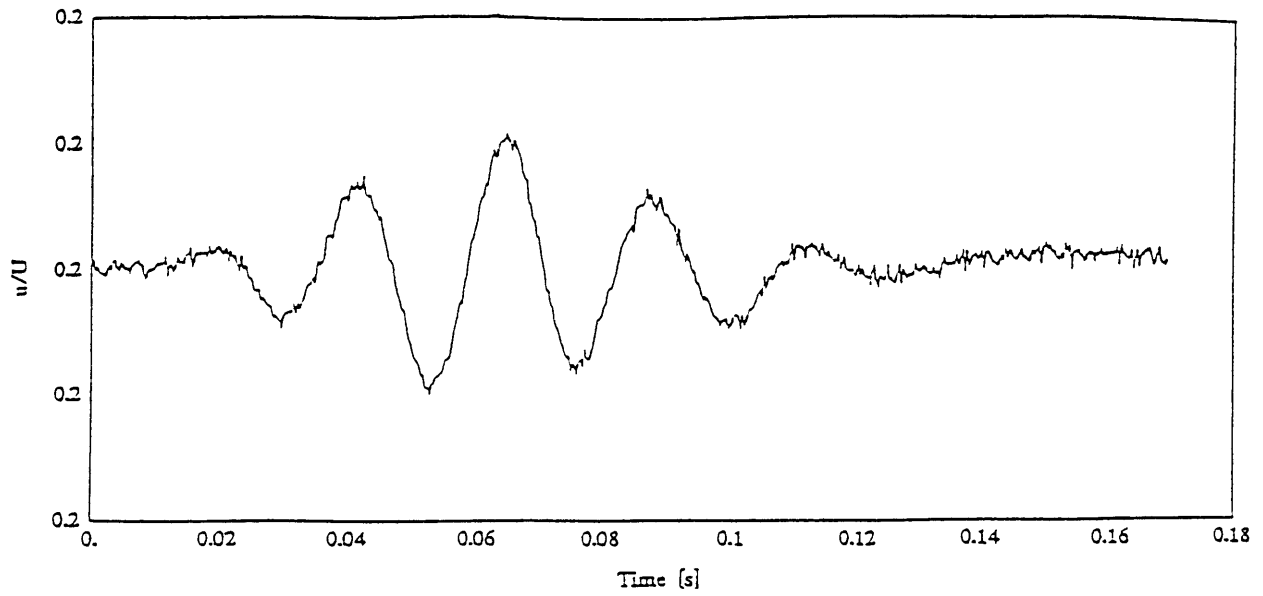
Figure 11 e. Positive disturbance. $x / \delta^* = 410$
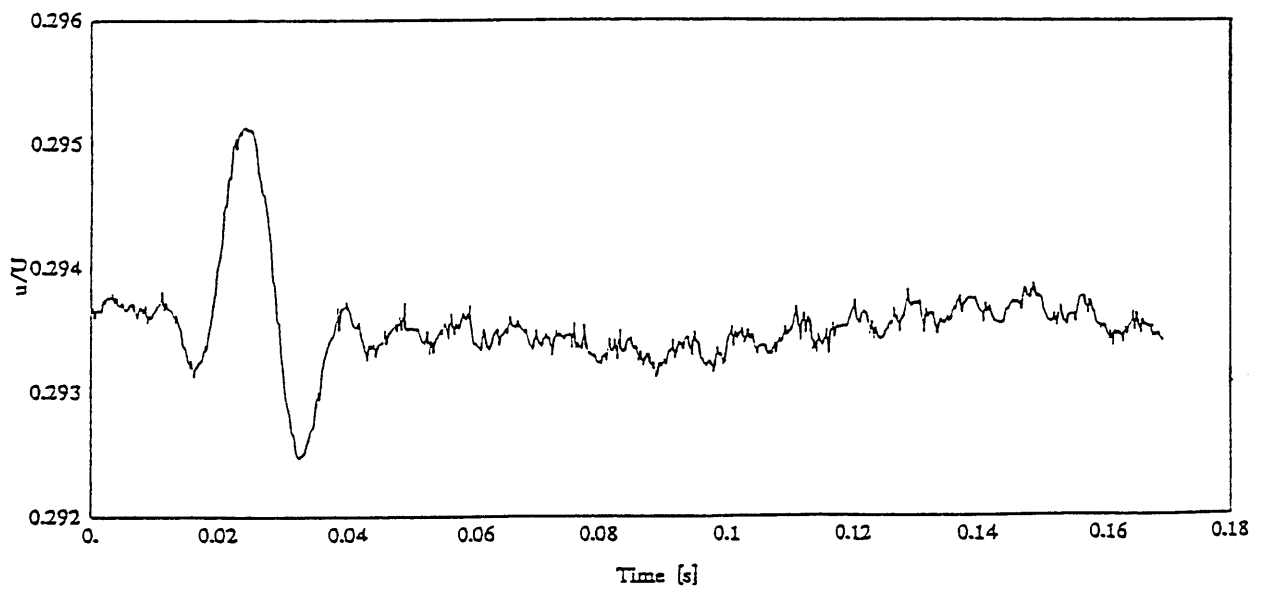
Figure 12 a. Negative disturbance. $x / \delta^* = 25$
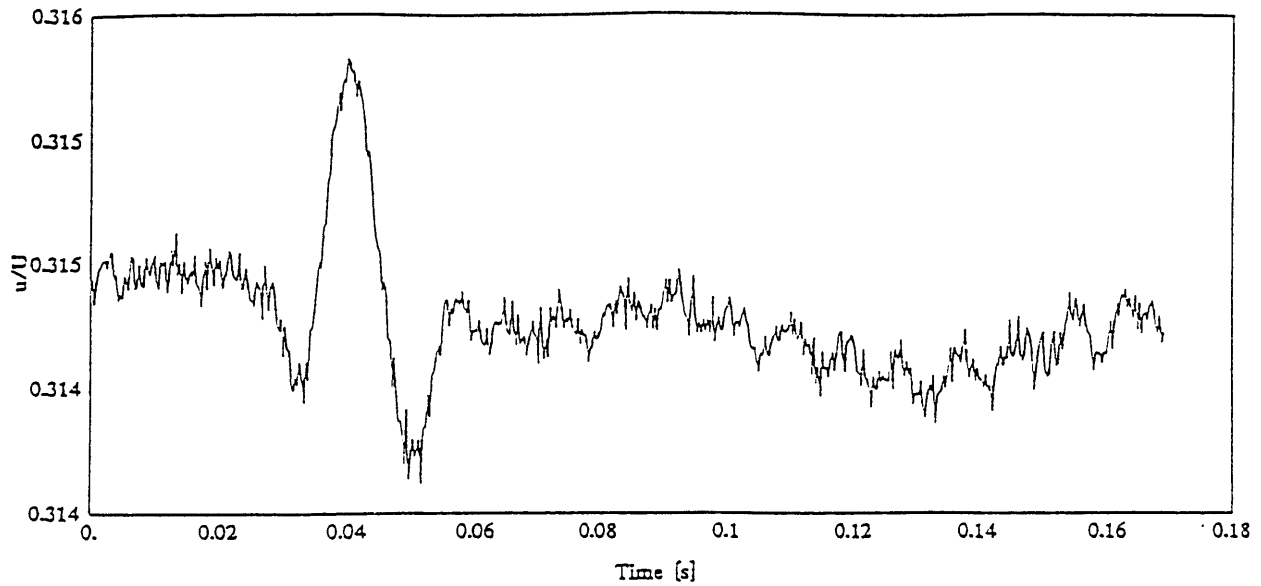
Figure 12 b. Negative disturbance. $x / \delta^* = 50$
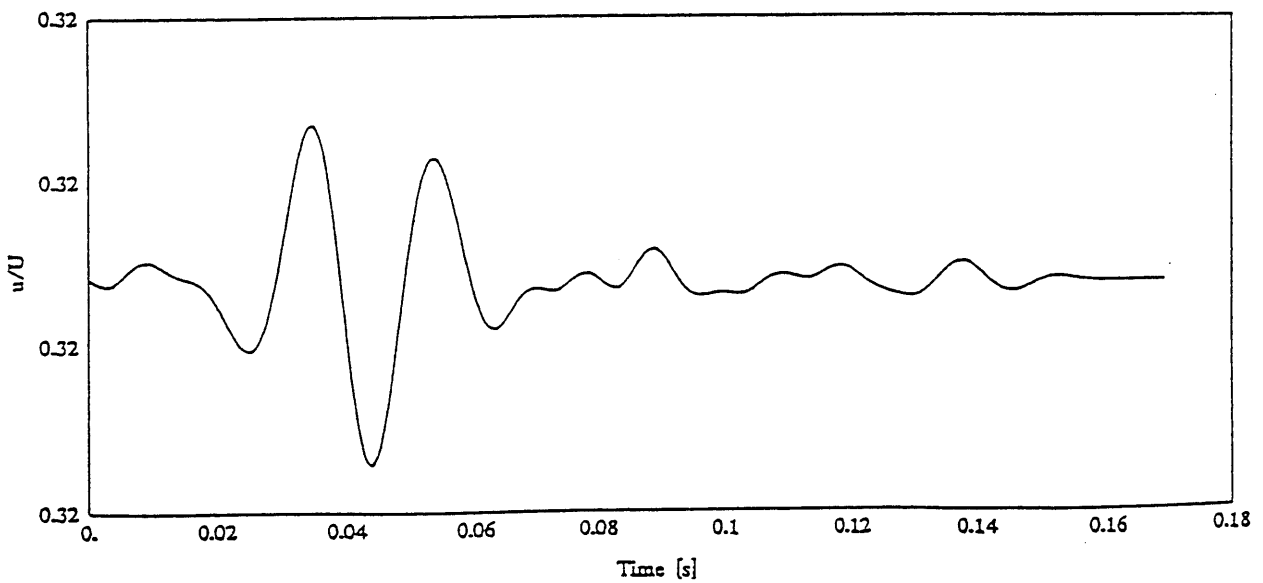
Figure 12 c. Negative disturbance. $x / \delta^* = 97$, band–pass filtered signal.
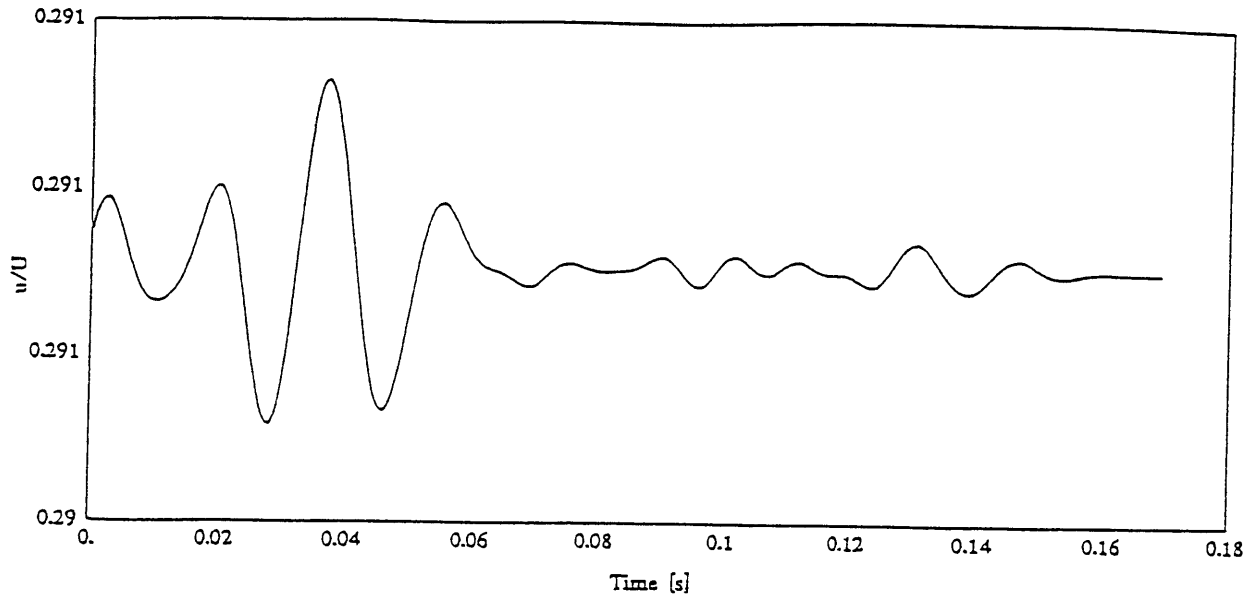
Figure 12 d. Negative disturbance. $x / \delta^* = 145$, band-pass filtered signal.
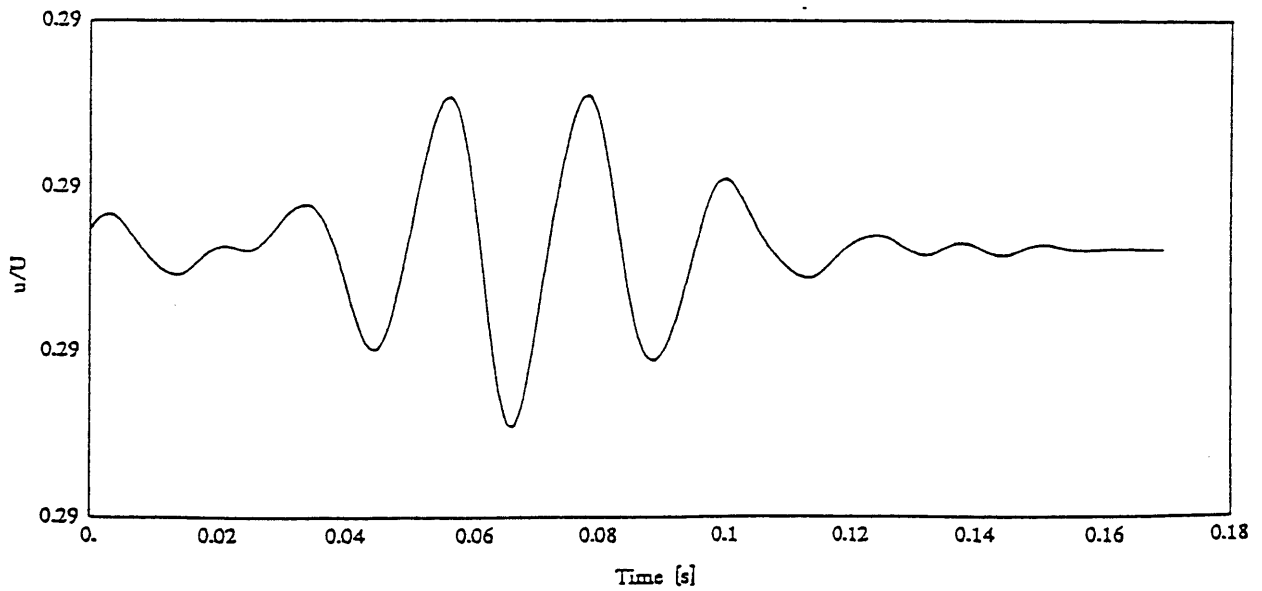
Figure 12 e. Negative disturbance. $x / \delta^* = 335$, band-pass filtered signal.
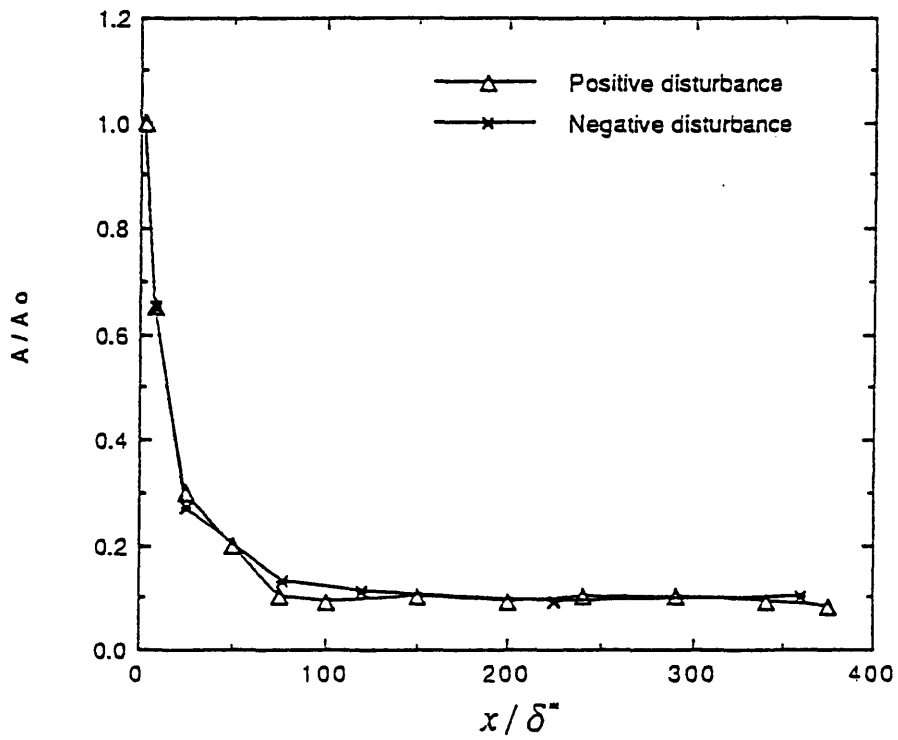
Figure 13 a. Amplitude of disturbance along the plate.
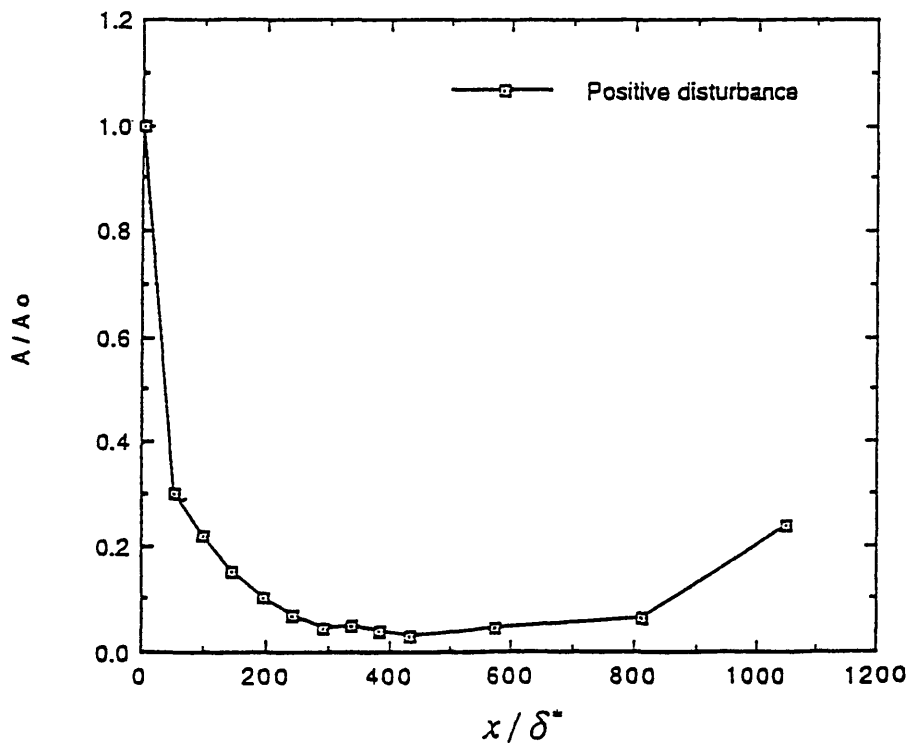
Figure 13 b. Positive disturbance amplitude developement downstream.
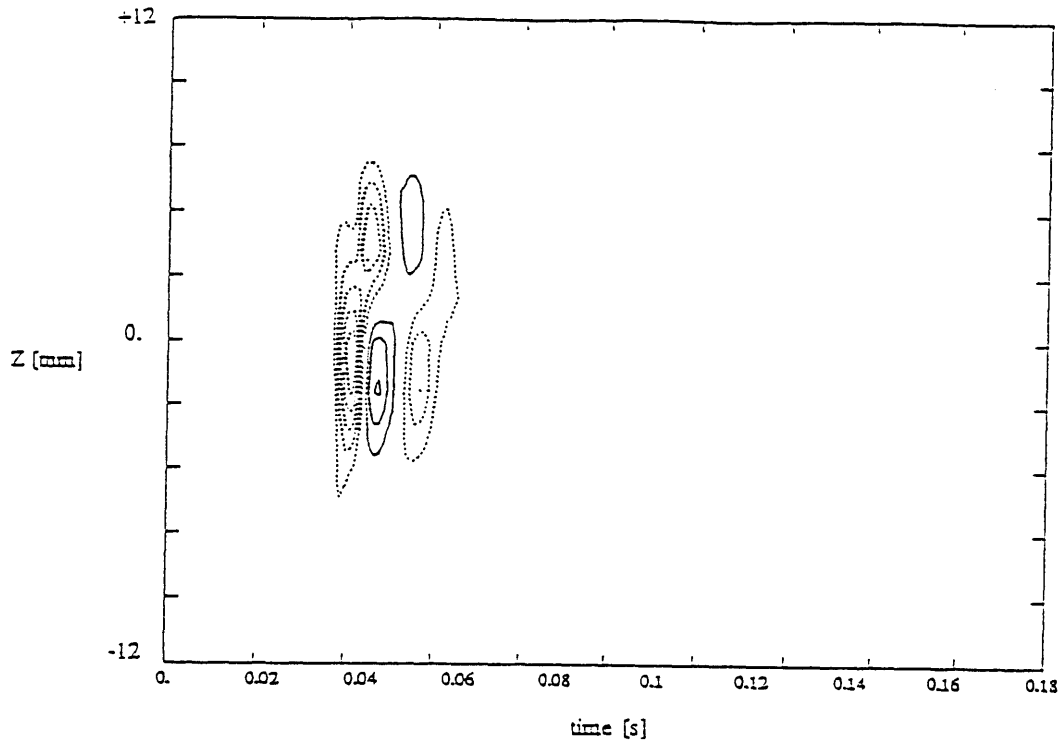
Figure 14 a. Positive disturbance. $x/\delta^* = 12$
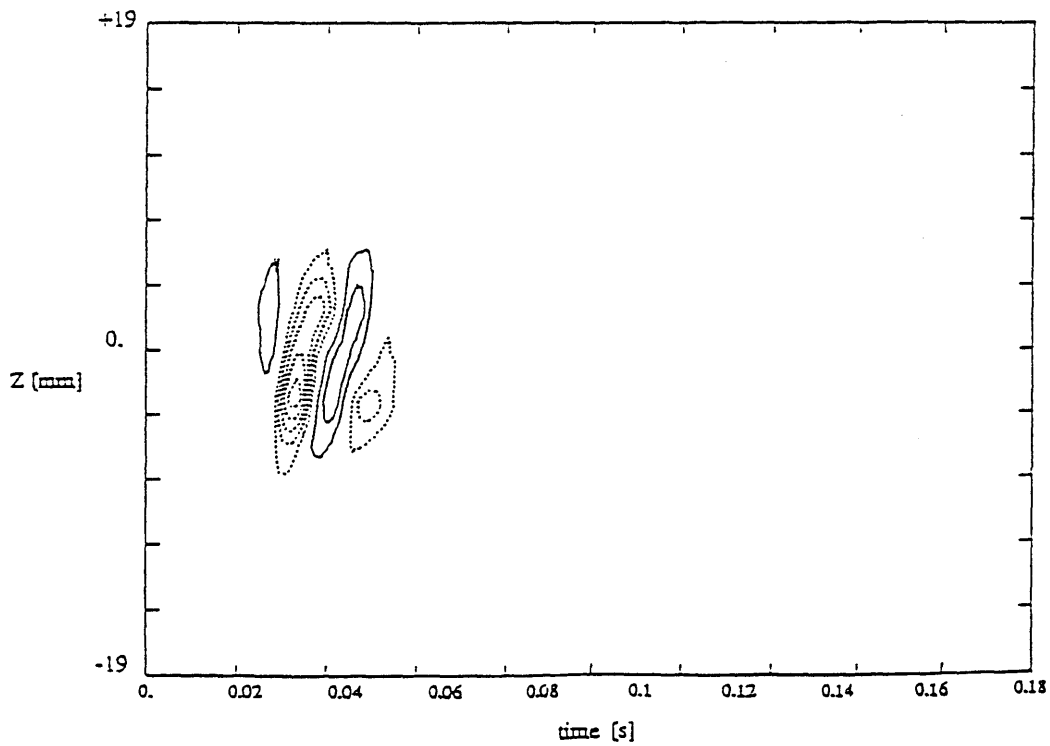
Figure 14 b. Positive disturbance. $x/\delta^* = 26$
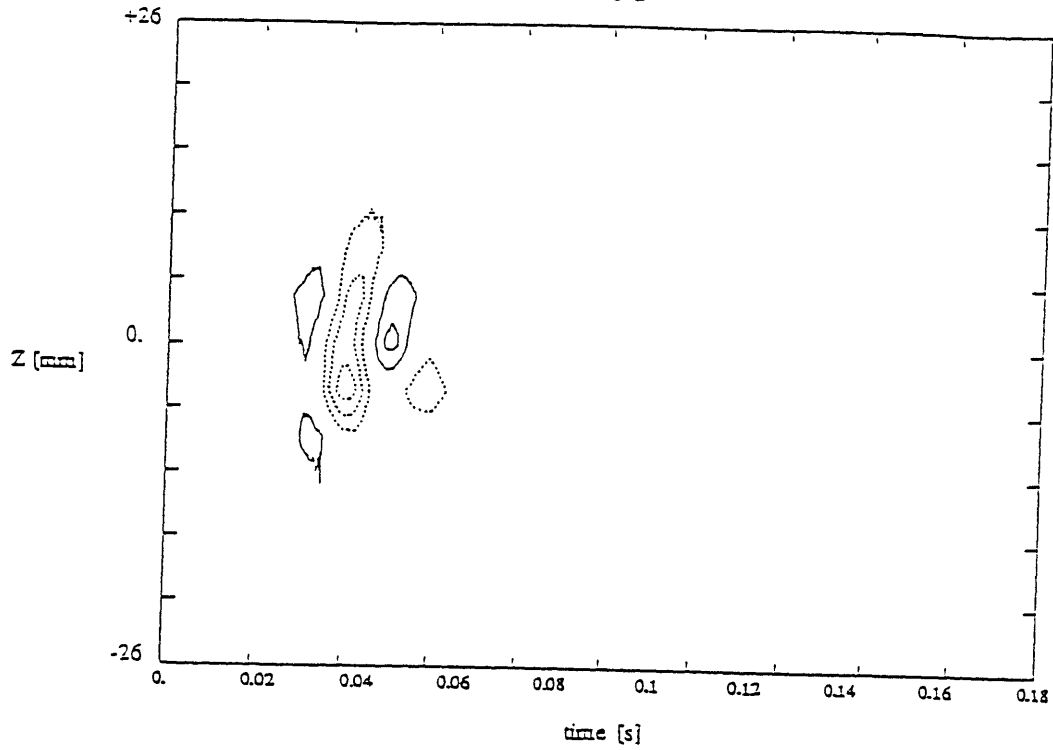
Figure 14 c. Positive disturbance. $x/\delta^* = 50$
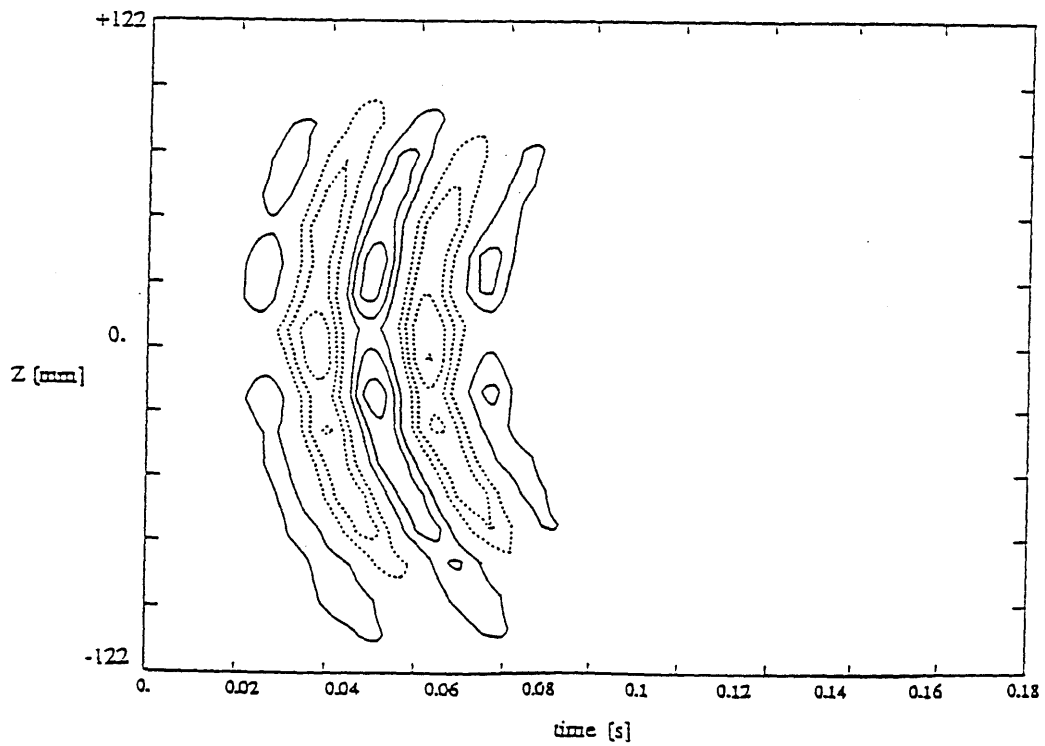
Figure 14 d. Positive disturbance. $x/\delta^* = 240$, band-pass filtered signal.
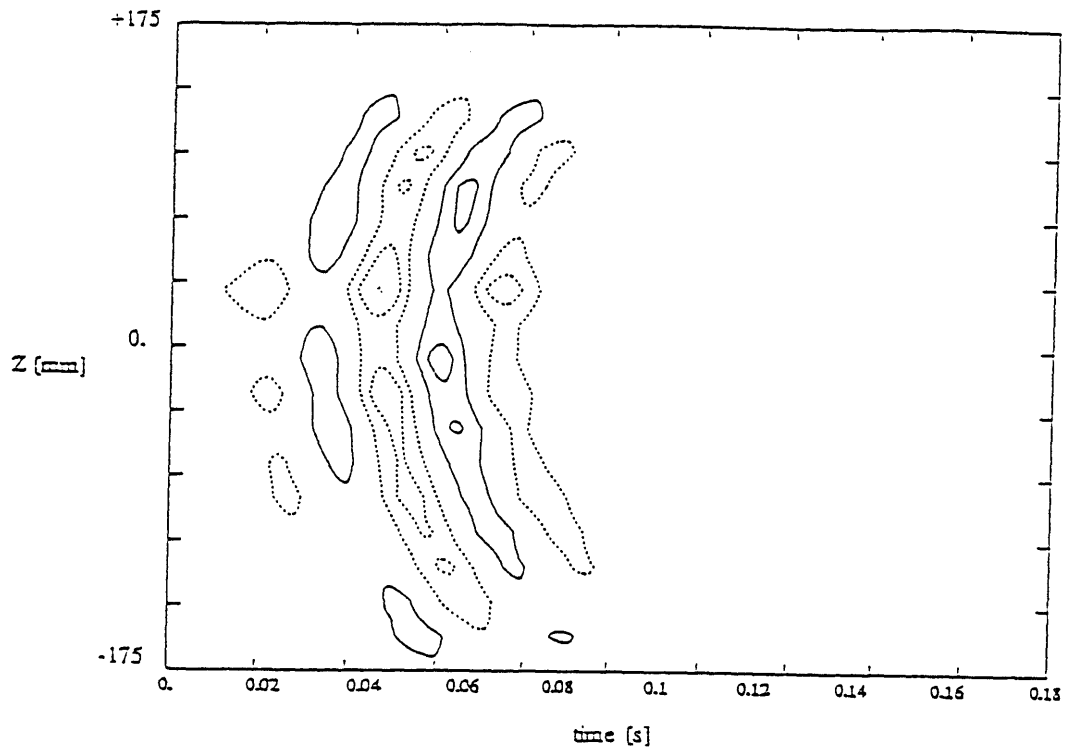
Figure 14 e. Positive disturbance. $x / \delta^{*} = 335$, band-pass filtered signal.
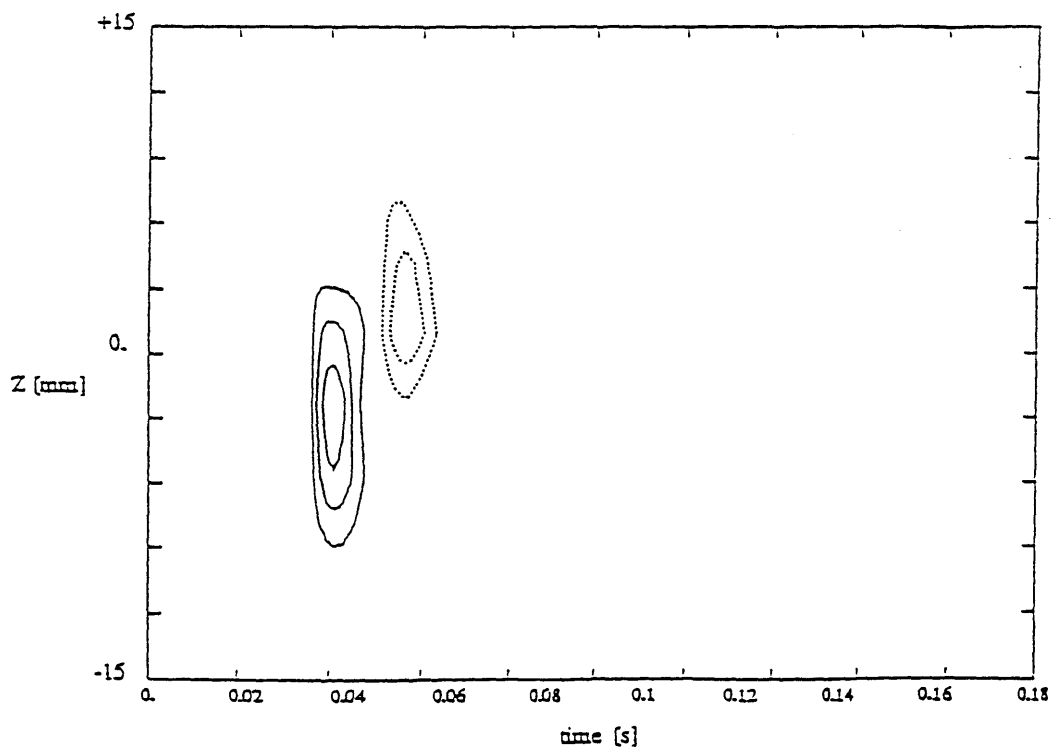
Figure 15 a. Negative disturbance. $x / \delta^{*} = 22$
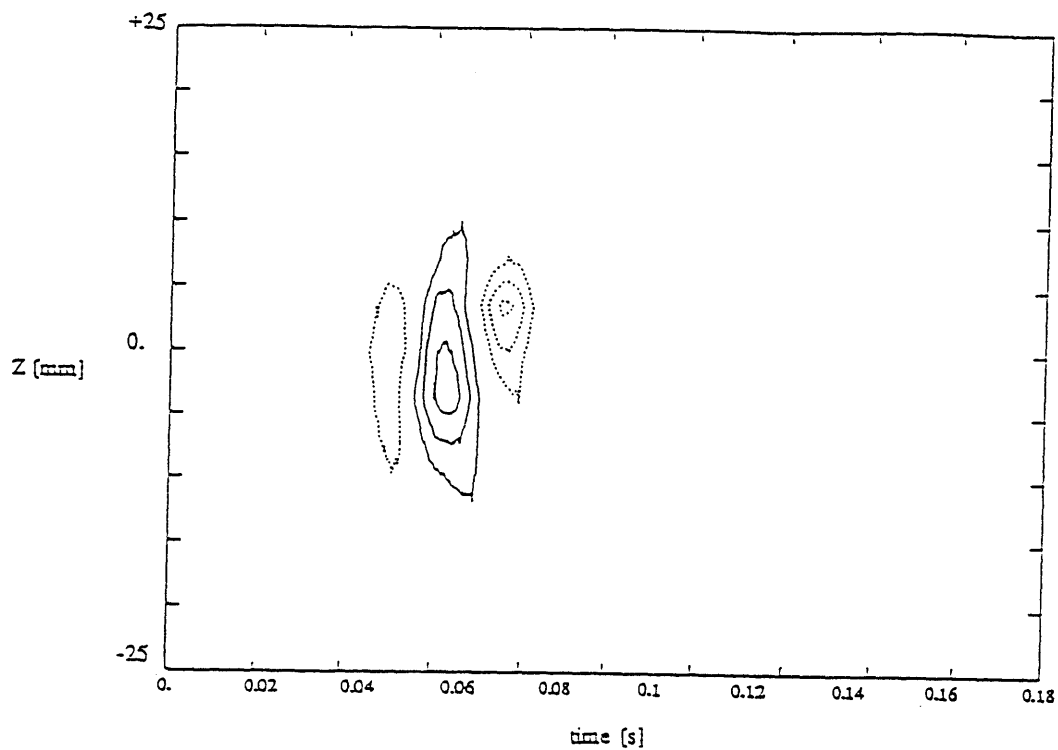
Figure 15 b. Negative disturbance. $x / \delta^* = 50$
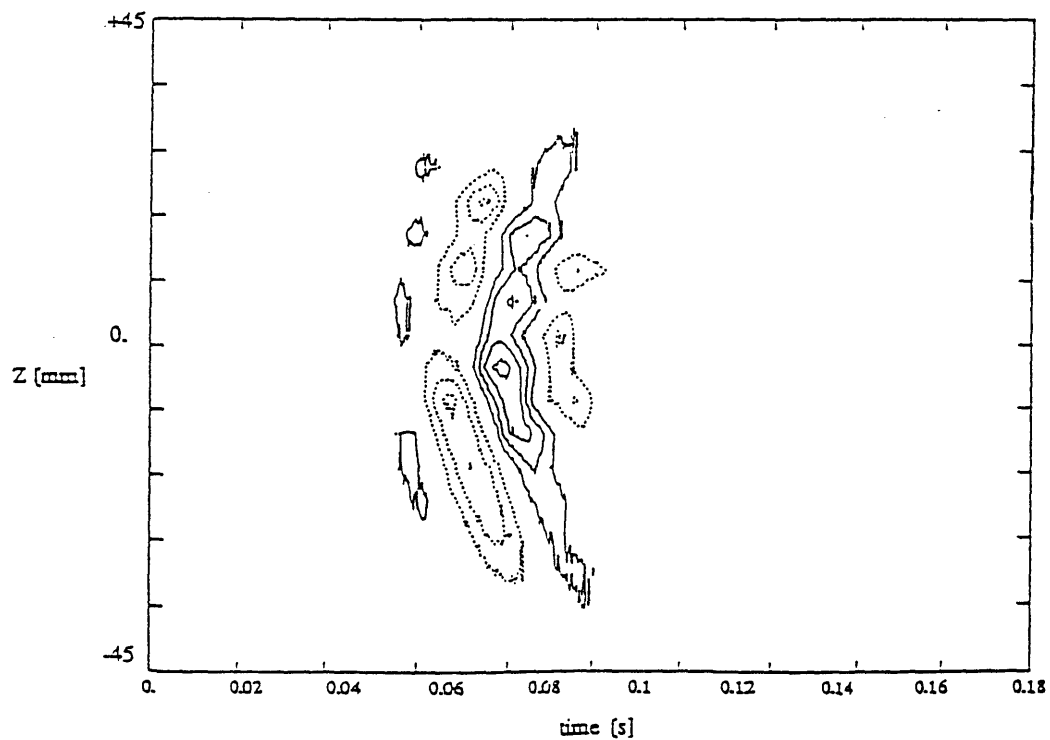
Figure 15 c. Negative disturbance. $x / \delta^* = 97$
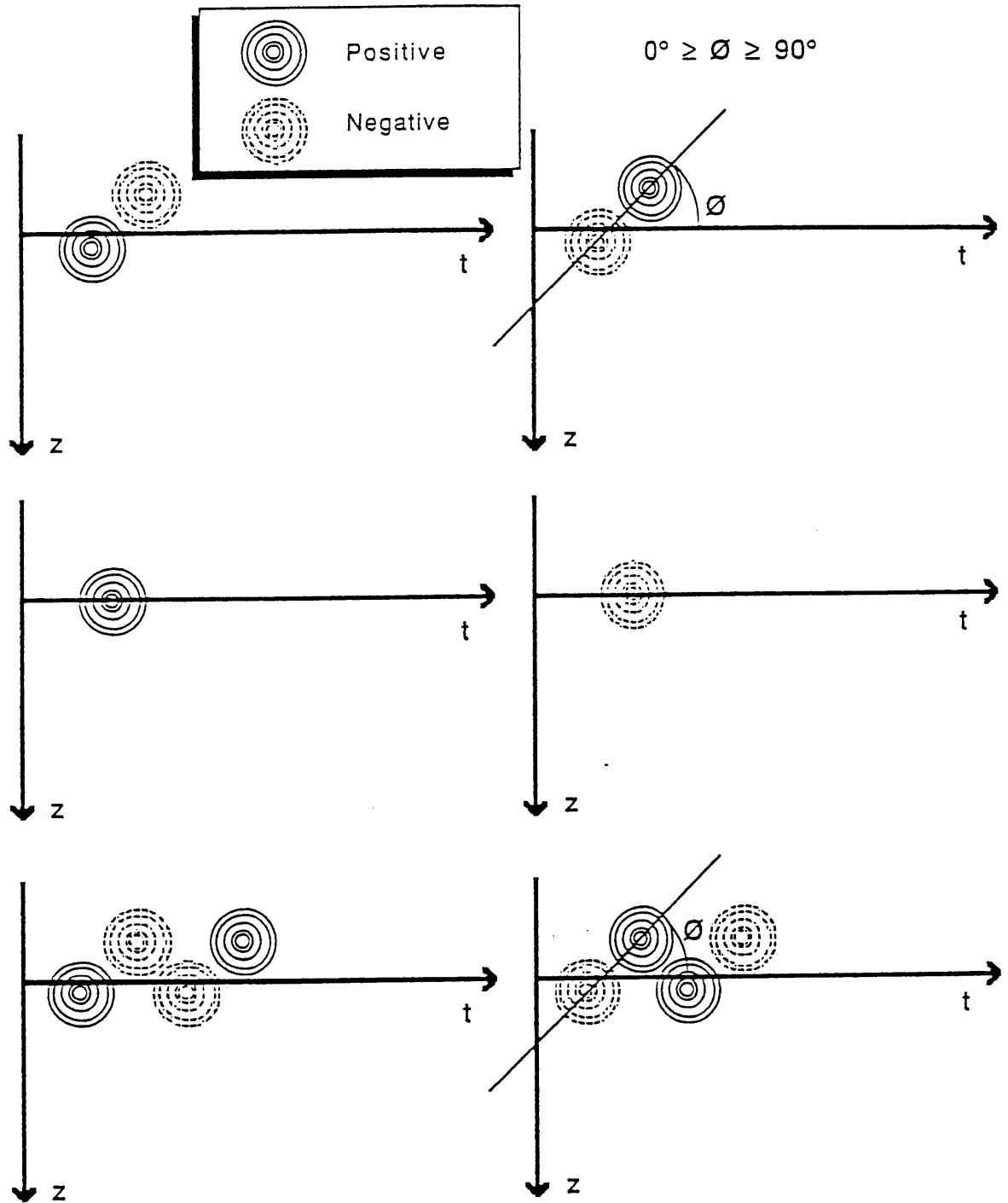
Figure 16. Examples of initial disturbances.
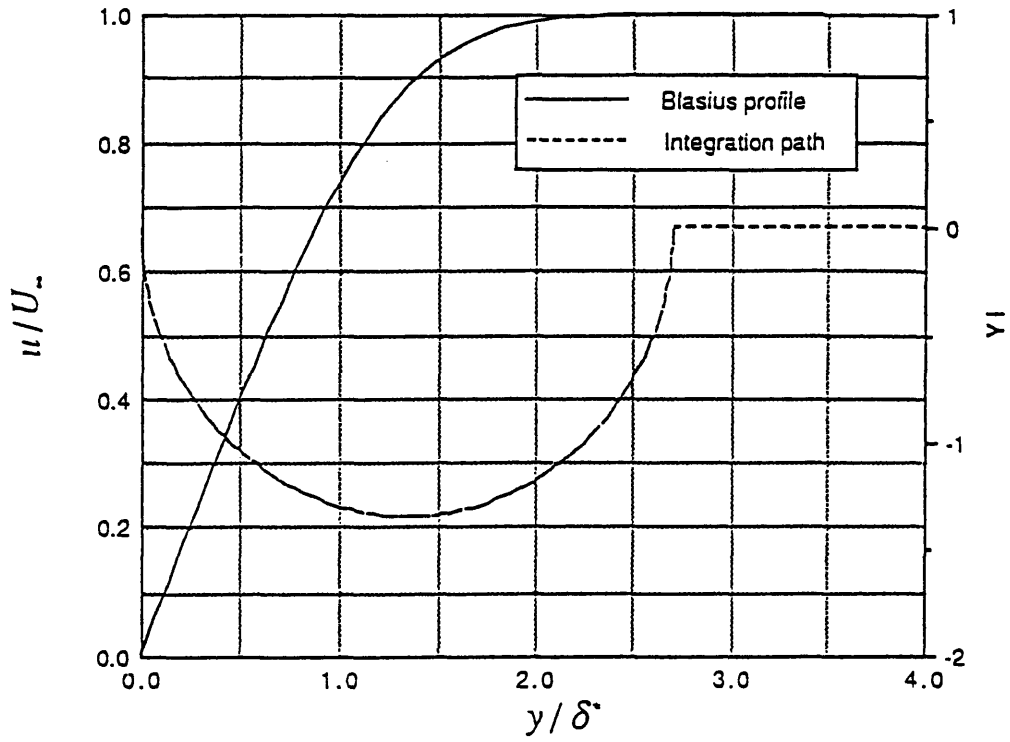
Figure 17. Integration path for solving Rayleigh equation for the Blasius boundary layer.
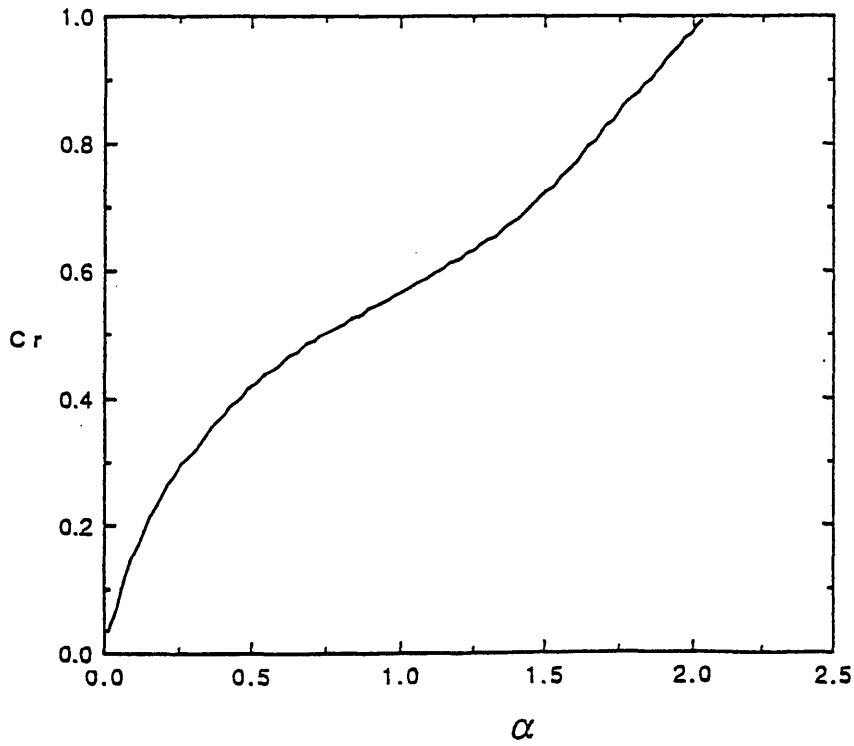
Figure 18 a. Phase speed as function of wave number.
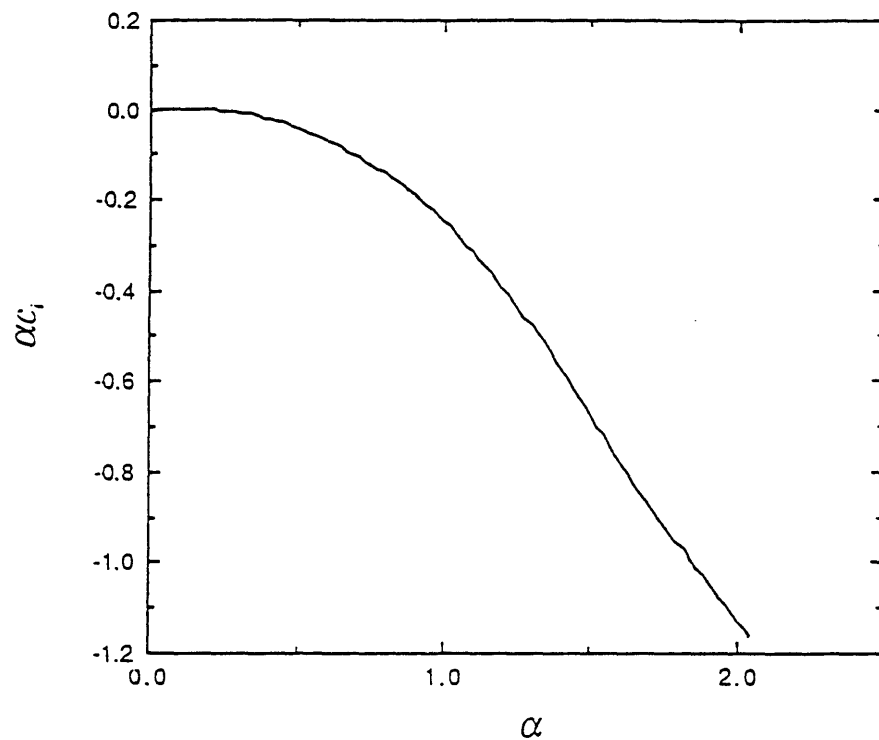
Figure 18 b. Damping factor as function of wave number.
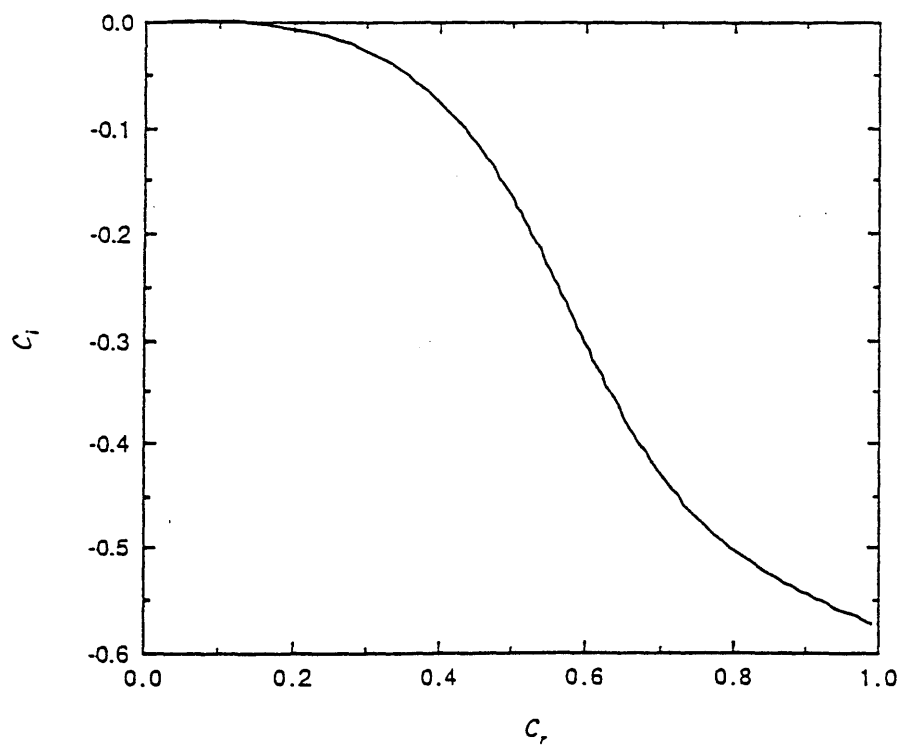
Figure 18 c. Inviscid eigenvalues of the Blasius boundary layer.